Stem Cell Reports
Article

ISSCR

OPEN ACCESS

Synergic Functions of miRNAs Determine Neuronal Fate of Adult Neural Stem Cells

Meritxell Pons-Espinal,[1] Emanuela de Luca,[1] Matteo Jacopo Marzi,[2] Ruth Beckervordersandforth,[3] Andrea Armirotti,[4] Francesco Nicassio,[2] Klaus Fabel,[5,6] Gerd Kempermann,[5,6] and Davide De Pietri Tonelli[1,*]

[1]Neurobiology of miRNA Lab, Neuroscience and Brain Technologies Department, Istituto Italiano di Tecnologia, Via Morego 30, 16163 Genoa, Italy
[2]Center for Genomic Science, Istituto Italiano di Tecnologia, IFOM-IEO CAMPUS, Via Adamello 16, 20139 Milan, Italy
[3]Institute of Biochemistry, Emil Fischer Center, Friedrich-Alexander-Universität Erlangen-Nürnberg, 91054 Erlangen, Germany
[4]D3 PharmaChemistry, Department of Drug Discovery and Development, Fondazione Istituto Italiano di Tecnologia, Via Morego 30, 16163 Genoa, Italy
[5]German Center for Neurodegenerative Diseases (DZNE) Dresden, Arnoldstraße 18/18b, 01307 Dresden, Germany
[6]CRTD – Center for Regenerative Therapies Dresden, Technische Universität Dresden, Fetscherstraße 105, 01307 Dresden, Germany
*Correspondence: davide.depietri@iit.it
http://dx.doi.org/10.1016/j.stemcr.2017.02.012

SUMMARY

Adult neurogenesis requires the precise control of neuronal versus astrocyte lineage determination in neural stem cells. While microRNAs (miRNAs) are critically involved in this step during development, their actions in adult hippocampal neural stem cells (aNSCs) has been unclear. As entry point to address that question we chose DICER, an endoribonuclease essential for miRNA biogenesis and other RNAi-related processes. By specific ablation of *Dicer* in aNSCs in vivo and in vitro, we demonstrate that miRNAs are required for the generation of new neurons, but not astrocytes, in the adult murine hippocampus. Moreover, we identify 11 miRNAs, of which 9 have not been previously characterized in neurogenesis, that determine neurogenic lineage fate choice of aNSCs at the expense of astrogliogenesis. Finally, we propose that the 11 miRNAs sustain adult hippocampal neurogenesis through synergistic modulation of 26 putative targets from different pathways.

INTRODUCTION

Neural stem cells (NSCs) resident in the two main neurogenic niches of the adult mammalian brain (the subventricular zone [SVZ] of the lateral ventricle and the subgranular zone of the hippocampal dentate gyrus [DG]) are two heterogeneous populations of radial glia-like precursor cells that have astrocytic properties, express bona fide stem cell markers and rarely divide. These cells have the capacity to self-renew and differentiate, giving rise to both neurons and glia (reviewed in Bond et al., 2015; Kempermann et al., 2015). The mechanisms of fate determination in adult hippocampal NSC (aNSC) lineage is a highly debated topic (Bonaguidi et al., 2012; Kempermann, 2011) and of fundamental importance. In addition, understanding the molecular mechanisms underlying lineage determination might provide new avenues to prevent age-dependent loss of neurogenesis (Encinas et al., 2011; Marlatt and Lucassen, 2010; Pons-Espinal et al., 2013), or the pathological generation of undesirable cells such as activated glia upon trauma and epilepsy (Dibajnia and Morshead, 2013; Doetsch et al., 2002; Shimada et al., 2012; Sierra et al., 2015).

Regulation of aNSC fate determination is known to be possible at the transcriptional level (Beckervordersandforth et al., 2015), but accumulating evidence indicates that additional control layers, such as epigenetics and non-coding RNAs, are involved in this mechanism (Castel and Martienssen, 2013; Cernilogar et al., 2011; Huang and Li, 2014; Li, 2014; Noguchi et al., 2015; Schouten et al., 2012). MicroRNAs (miRNAs) are small (~22 nt long) single-stranded non-coding RNAs, which post-transcriptionally repress target mRNAs through imperfect miRNA-mRNA binding (Agarwal et al., 2015; Ha and Kim, 2014; Krol et al., 2010). They exert their regulatory functions in a highly combinatorial way: one miRNA can regulate several mRNAs in parallel (Lim et al., 2005), and different miRNAs can target one mRNA simultaneously, thus repressing its expression more efficiently (Selbach et al., 2008). Based on these observations, miRNAs are predicted to regulate the majority of mammalian mRNAs (Friedman et al., 2009).

Despite the known functions of miRNAs in fate determination of embryonic and adult SVZ NSCs (Barca-Mayo and De Pietri Tonelli, 2014; Cheng et al., 2009; Zhao et al., 2009), as well as survival and dendritic maturation of adult-born neurons in the DG (Konopka et al., 2010; Magill et al., 2010; Schouten et al., 2015; Smrt et al., 2010), it has been unknown whether miRNAs regulate neuronal versus astrocyte lineage fate determination in the adult hippocampus. Indeed, as single miRNAs could have opposite effects depending on the spatiotemporal expression of their targets (Zhu et al., 2011), it is possible to hypothesize that the same miRNAs might exert different functions in various cell types involved in adult hippocampal neurogenesis.

Current approaches to infer miRNA functions in vivo either manipulate single miRNAs/targets or deplete miRNAs by conditional knockouts of genes encoding essential miRNA biogenesis proteins such as DROSHA,

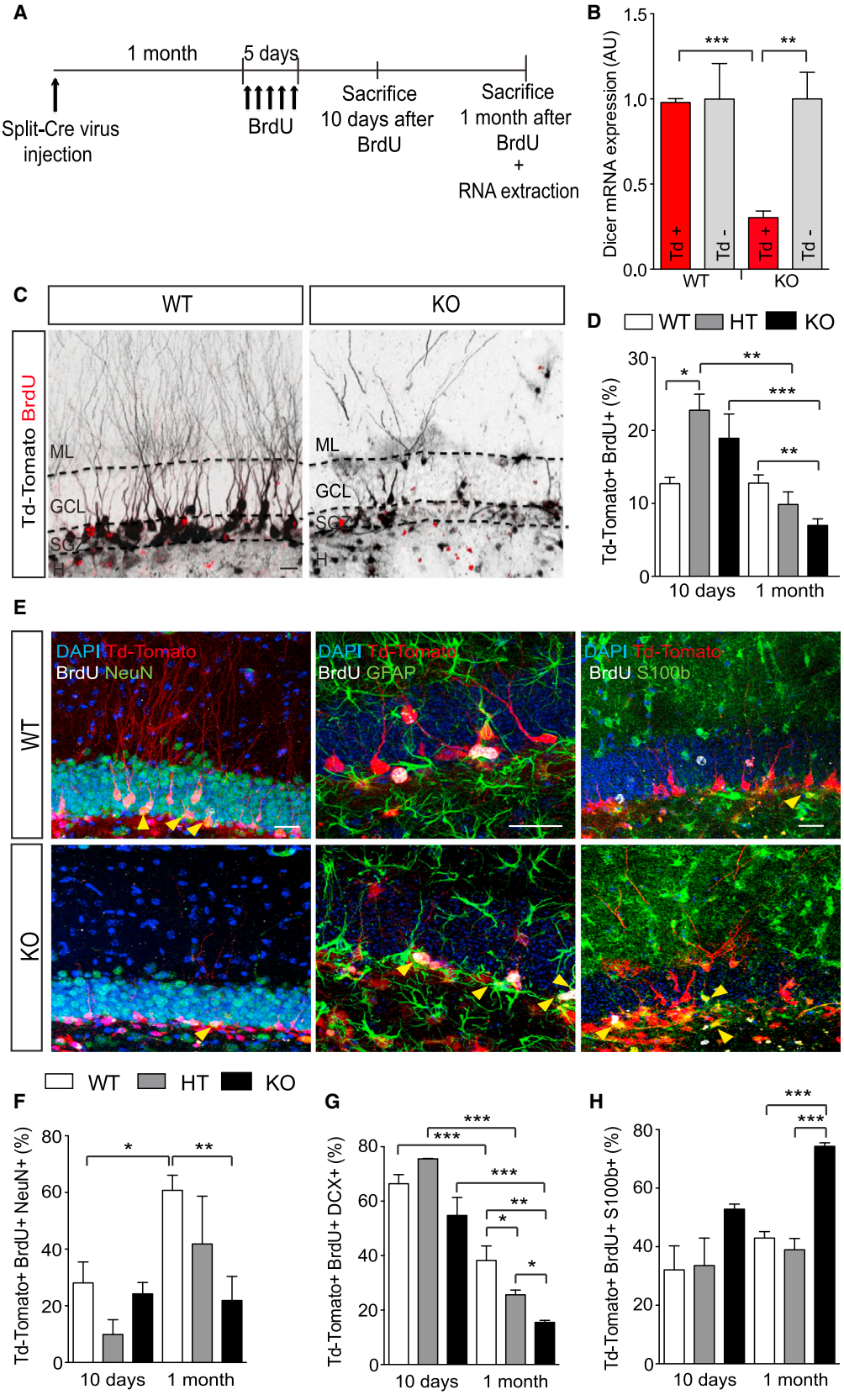

(legend on next page)

DGCR8, or DICER. Although both approaches successfully demonstrated critical functions for specific miRNAs and miRNA biogenesis proteins in neurogenesis (Aksoy-Aksel et al., 2014; Barca-Mayo and De Pietri Tonelli, 2014; Schouten et al., 2012), most of these studies neglected the intrinsic combinatorial nature of miRNA-dependent control (Schmiedel et al., 2015; Siciliano et al., 2013), or left unresolved the question of miRNA-specific versus miRNA-independent functions of miRNA biogenesis proteins (Yang and Lai, 2011).

By conditional ablation of *Dicer* specifically in bona fide aNSCs of the adult hippocampus in vivo and in vitro and by manipulation of specific miRNAs, here we studied the role of miRNAs for lineage fate choice of aNSCs. Our study identified a set of 11 miRNAs that, by synergistic enforcement of gene-regulatory networks, allows aNSCs to acquire the neurogenic fate at the expense of astrogliogenesis.

RESULTS

Split-Cre Virus-Mediated *Dicer* Ablation In Vivo Impairs Neurogenesis, but Not Astrogliogenesis, in the Adult Hippocampus

To study the role of DICER in adult hippocampal neurogenesis in vivo, we first crossed a mouse line carrying a conditional allele for *Dicer* (*Dicer*^{flox}, Murchison et al., 2005) with a Cre-inducible reporter mouse line (Td-Tomato^{flox}, Madisen et al., 2010). To achieve conditional ablation of *Dicer* and expression of Tomato in bona fide type 1 aNSCs, we injected split-Cre viruses (allowing specific expression of an active Cre recombinase in type 1 aNSCs, based on the coincident activity of human glial fibrillary acidic protein [hGFAP] and Prominin1 promoters) (Figures 1A and S1A; Beckervordersandforth et al., 2014) in the DG of 8-week-old *Dicer*$^{wt/wt}$ Td-Tomato$^{flox/wt}$ (wild-type; WT), *Dicer*$^{flox/wt}$ Td-Tomato$^{flox/wt}$ (Dicer HT), and *Dicer*$^{flox/flox}$ Td-Tomato$^{flox/wt}$ (Dicer cKO) mice, and followed the fate of the labeled cells in the subgranular zone (SGZ) and granule cell layer (GCL) of the hippocampus.

To ascertain *Dicer* ablation in vivo, we sorted Tomato$^+$ cells by fluorescence-activated cell sorting (FACS) and, as internal control non-infected Tomato$^-$ cells, from the DG of WT and *Dicer* cKO mice, and quantified *Dicer* mRNA levels by quantitative real-time PCR (qRT-PCR). This quantification confirmed a 70% reduction of *Dicer* mRNA levels in Tomato$^+$ cells from *Dicer* cKO mice, compared with Tomato$^+$ cells from WT mice (Figure 1B, $p = 0.0001$) and Tomato$^-$ cells from both WT and *Dicer* cKO mice (Figure 1B, $p = 0.003$).

To investigate the survival of the progeny originating from the *Dicer* cKO aNSCs at 1 month after virus injection, we administered bromodeoxyuridine (BrdU) for 5 consecutive days. Ten days or 1 month after BrdU, we quantified the proportion of Tomato/BrdU double-positive cells in the SGZ/GCL of WT, *Dicer* HT, and cKO mice (Figure 1A). The proportion of Tomato/BrdU double-positive cells in *Dicer* cKO and *Dicer* HT mice showed a slight increase at 10 days (Figure 1D), but significantly decreased in *Dicer* cKO mice at 1 month (Figures 1C and 1D, $p = 0.006$). This result indicated that *Dicer* depletion impaired survival of newborn cells in the SGZ/GCL.

Moreover, we also observed a dramatic reduction in the number of processes and arborization of Tomato$^+$ *Dicer* cKO cells in the GCL and molecular layer (ML) of the hippocampus compared with Tomato$^+$ WT cells (Figure 1C). This finding suggested that *Dicer* depletion impaired the differentiation and maturation of the surviving cells.

Next, we assessed the role of DICER in neuronal fate choice. We quantified the proportion of newborn cells co-expressing the immature neuronal marker doublecortin (DCX) or postmitotic neuronal marker NeuN in the SGZ/GCL of the adult hippocampus of *Dicer* WT, HT, and cKO mice (as in Figure 1A). At 10 days we did not find differences in DCX and NeuN expression among the groups (Figures 1F and 1G). However, at 1 month we found that 40% of *Dicer* WT cells also co-expressed DCX, whereas only 26% of *Dicer* HT cells and 10% of *Dicer* cKO cells did so, respectively (Figure 1G, WT versus KO, $p = 0.0012$; WT versus HT, $p = 0.039$). Consistently, at the same age, only 20% of *Dicer* cKO cells co-expressed NeuN, compared with 60%

Figure 1. Split-Cre Virus-Mediated *Dicer* Ablation In Vivo Impairs Neuronal Differentiation and Survival but Not Astrogliogenesis

(A) Schematic representation of the experiment.

(B) qRT-PCR quantification of *Dicer* mRNA from FACS-sorted Td-Tomato$^+$ aNSCs 2 months after split-Cre virus injection.

(C and E) Representative micrographs showing recombined Td-Tomato/BrdU double-positive cells from *Dicer* WT and *c*KO mice 1 month after BrdU injection (C), co-expressing NeuN (E, left panel), GFAP (E, middle panel) and S100b (E, right panel). Yellow arrowheads show Td-Tomato/BrdU double-positive cells co-expressing NeuN, GFAP, or S100b.

(D) Percentage of Td-Tomato$^+$ cells expressing BrdU after 10 days, or 1 month after BrdU injections.

(F–H) Percentage of Td-Tomato/BrdU double-positive cells co-expressing NeuN (F), DCX (G), or S100b (H) 10 days or 1 month after BrdU injections.

ML, molecular layer; GCL, granular cell layer; SGZ, subgranular zone; H, Hilus. Data are expressed as mean ± SEM, n = 4–6 mice per group. Unpaired t test was used for Dicer mRNA expression analysis. One-way ANOVA Bonferroni as post hoc was used to analyze cell marker quantification. *$p < 0.05$, **$p < 0.01$, ***$p < 0.001$. Scale bars, 20 μm.

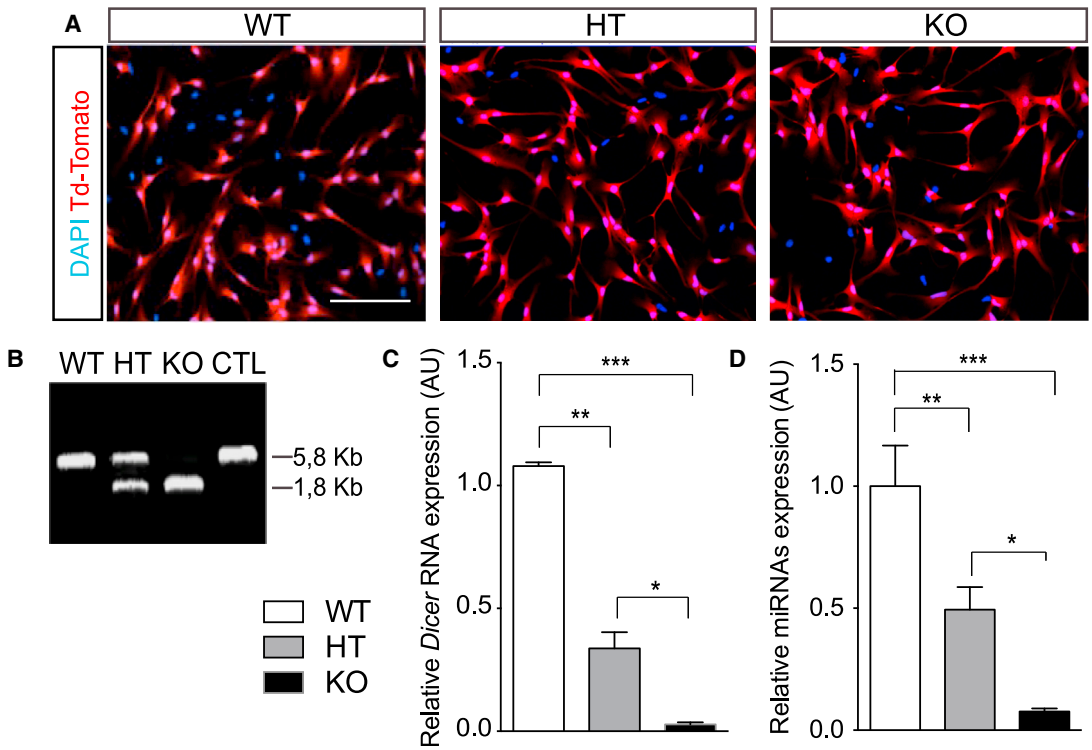

Figure 2. *Dicer* and miRNAs Are Depleted after Recombination of *Dicer*^{flox} Allele in Hippocampal aNSCs In Vitro

(A) Representative micrographs showing Td-Tomato^{+} aNSCs from *Dicer* WT, *Dicer* HT, and *Dicer* cKO mice after nucleofection with Cre recombinase.

(B) PCR Genotyping of Cre-recombined aNSCs, showing the three *Dicer* genotypes.

(C) qRT-PCR quantification of *Dicer* mRNA in Cre-recombined aNSCs.

(D) Average of all miRNAs quantified from recombined aNSCs.

Data are expressed as mean ± SEM, n = 3 independent experiments containing three replicates. One-way ANOVA Bonferroni as post hoc: *p < 0.05, **p < 0.01, ***p < 0.001. Scale bar, 50 μm.

of NeuN^{+} *Dicer* WT neurons (Figures 1E and 1F, p = 0.0058). Moreover, although the proportion of newborn NeuN^{+} neurons increased significantly between 10 days and 1 month in the SGZ/GCL of *Dicer* WT mice (Figures 1E and 1F, p = 0.0062), this population did not grow over time in *Dicer* cKO mice (p = 0.72). These results indicate that *Dicer* depletion impairs neuronal differentiation and maturation in the adult mouse hippocampus in vivo.

We then assessed the role of DICER on adult astrogliogenesis by immunostaining for three different astrocyte markers, GFAP, S100b (Figure 1E), and glutamine synthetase (GS; Figure S1B) and found results complementary to the findings on neurogenesis. Whereas no significant differences were observed for S100b at 10 days between the three *Dicer* genotypes; at 1 month the proportion of S100b^{+} (Figure 1H, p = 0.0002) and GS^{+} (Figure S1C, p = 0.024) was about twice as high in the SGZ/GCL of *Dicer* cKO mice than in controls. Moreover, upon *Dicer* ablation we did not observe an increase in progenitor markers such as Nestin or SOX2 (Figures S1B and S1C), largely excluding the possibility that *Dicer* cKO cells remained in undifferentiated or quiescent state. Thus, these results indicated that *Dicer* depletion in type 1 aNSCs impaired neurogenesis and favored astrogliogenesis in the adult hippocampus in vivo.

Loss of DICER-Dependent miRNAs Does Not Affect aNSC Proliferation and Stemness, but Increases Apoptosis upon Their Differentiation In Vitro

To ascertain the effect of *Dicer* ablation in vitro, we generated primary aNSCs from the DG of mice WT, HT, and homozygous for *Dicer*^{flox} allele, which were also heterozygous for the Cre-inducible Td-Tomato allele, by culturing them in monolayers (Figure S1D) as described previously (Babu et al., 2011; Walker and Kempermann, 2014). Upon recombination of *Dicer*^{flox} locus (Figure 2B) and expression of Tomato protein (Figure 2A), we saw a 50% reduction of *Dicer* transcript in *Dicer* HT aNSCs (Figure 2C, p = 0.0082) and almost total loss in *Dicer* cKO aNSCs (Figure 2C,

p = 0.0003) compared with WT. Consequently, mature miRNAs levels were reduced to 50% in *Dicer* HT aNSCs (Figure 2D, p = 0.01) and almost completely depleted in *Dicer* cKO aNSCs (Figure 2D, residual miRNA levels 7%; p < 0.0001), compared with WT cells. These results demonstrated that recombination of the $Dicer^{flox}$ allele resulted in efficient depletion of both *Dicer* transcript and mature miRNAs from hippocampal aNSCs in vitro. Despite efficient loss of DICER-dependent miRNAs, we were able to keep *Dicer* cKO aNSCs in culture under proliferative conditions for at least 18 days in vitro (DIV). We did not detect major differences in cell morphology or passaging requirements for cells from the three genotypes. Moreover, no differences were observed in the percentage of $Tomato^+$ cells incorporating BrdU after a 2-hr pulse (Figures S2A–S2C and S2G–S2I), or pH3 (Figures S2D and S2E). Consistently, the growth curve was unchanged over several days in culture (Figure S2F). Thus, we concluded that loss of DICER-dependent miRNAs does not affect aNSCs proliferation.

Next, we investigated stem cell markers SOX2, GFAP, and Nestin in aNSCs, and found no change in SOX2 or GFAP expression at both protein and transcript levels in aNSCs from the three genotypes (Figure S3). However, consistent with our in vivo results (Figures S1B and S1C), we detected reduced expression of Nestin in *Dicer* cKO aNSCs compared with WT aNSCs (Figures S3A–S3C, p = 0.0021; Figure S3D, WT versus cKO p = 0.0053; HT versus cKO p = 0.03). Altogether, these results confirmed that loss of DICER-dependent miRNAs did not primarily affect proliferation, passaging requirements, and expression of stem cell markers of aNSCs. These results are consistent with previous studies on other stem cells types (Murchison et al., 2005) including embryonic NSCs (Andersson et al., 2010; De Pietri Tonelli et al., 2008), reporting that the effects of *Dicer* ablation are more prominent during cell fate transitions than in self-renewal.

Our data indicated that *Dicer* ablation impairs survival of newborn neurons in vivo (Figure 1). Thus we investigated the survival of aNSCs from *Dicer* WT, HT, and cKO upon induction of differentiation. Recombined ($Tomato^+$) *Dicer* WT, HT, and cKO aNSCs were FACS sorted, and equal numbers of aNSCs were seeded and cultivated under differentiating conditions (Figure S4A). After 6 DIV we found a 30% and 50% reduction in the number of *Dicer* HT and *Dicer* cKO aNSCs compared with WT aNSCs (Figures S4B and S4C, WT versus cKO, p = 0.03). Moreover, the reduced survival of *Dicer* cKO aNSCs was paralleled by a significant increase in the number of pycnotic nuclei (Figures S4B and S4C, p = 0.0051), expression of the apoptotic marker active-caspase-3 (Figures S4B and S4C, p = 0.013), and reduction in the expression of the transcript of anti-apoptotic protein Bcl-2 (Figure S4D, p = 0.04). Thus, consistently with in vivo data (Figure 1), these results indicated that DICER functions are not essential for expansion of aNSCs in vitro, but are required for survival of their progeny.

Loss of DICER-Dependent miRNAs Impairs Neurogenesis but Not Astrogliogenesis In Vitro

Our in vivo data suggested that *Dicer* depletion in aNSCs impairs neurogenesis but not astrogliogenesis in the adult mouse hippocampus (Figure 1). Thus, we isolated recombined ($Tomato^+$) *Dicer* WT, HT, and cKO aNSCs and investigated neurogenesis and neuronal maturation upon differentiation in vitro (Figure 3A). We found that *Dicer* HT and cKO aNSCs generated significantly fewer DCX^+ cells compared with WT aNSCs (Figures 3B and 3C, DCX^+ ~12% in *Dicer* HT, p = 0.04; ~9% in *Dicer* cKO, p = 0.0013). Moreover, we saw a reduction in the number of neurites, branch points, and dendritic spines in DCX^+ *Dicer* cKO cells compared with *Dicer* WT and HT cells (Figure 3D).

Next, we investigated astrogliogenesis in recombined ($Tomato^+$) *Dicer* WT, HT, and cKO aNSCs upon differentiation (as in Figure 3A) and found no difference between the three *Dicer* genotypes (Figure 6B). We then induced astrocyte differentiation with 10% fetal serum for 6 DIV (Figure 4A) and found no difference in the proportion of cells expressing astrocytic markers GFAP and S100b between groups (Figures 4B and 4C). These data were corroborated by a parallel decrease in the expression of the bona fide stem cell marker Nestin, at both mRNA and protein levels (Figures 4D–4H), and by a strong increase in the expression of astrocytic markers GFAP and S100b (Figures 4E, 4F, and 4I) in all genotypes. These results were consistent with our in vivo evidence (Figure 1) and indicated that DICER functions are essential for aNSC differentiation toward neurogenesis and neuronal maturation but not for astrogliogenesis.

A Pool of 11 miRNAs Determines aNSC Neurogenic Fate at the Expense of Astrogliogenesis

To clarify whether DICER-dependent miRNAs or additional RNAi-related functions of DICER are involved in the control of adult hippocampal neurogenesis, we first analyzed the dynamics of miRNA expression in WT aNSCs under proliferating conditions, as well as upon the induction of neuronal differentiation with virally transmitted ASCL1 expression at 7, 14, and 21 DIV (Figure 5A; Braun et al., 2013). This approach increased the proportion of $MAP2^+$ neurons to 95% (Figures S5A and S5B). By qRT-PCR we detected 335 mature miRNAs in these cells. These miRNAs could be classified into three groups according to the levels and dynamics of their expression during proliferation, early neuronal differentiation (7 DIV), and late neuronal differentiation (14 and 21 DIV) (Figure 5B). As expected, miRNAs known to be involved in proliferation or in neuronal differentiation were dynamically regulated

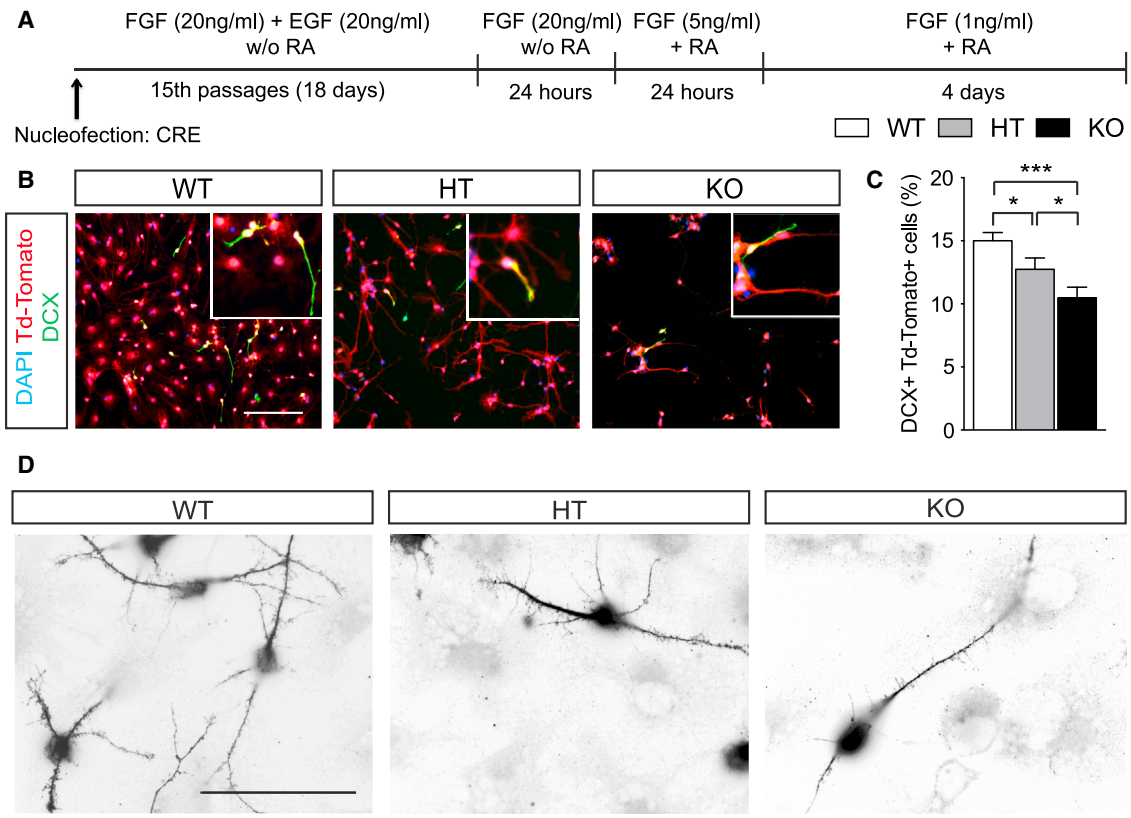

Figure 3. Loss of *Dicer*-Dependent miRNA in aNSCs Impairs Neurogenesis and Neuronal Maturation In Vitro

(A) Schematic representation of the protocol and experiment.

(B) Representative micrographs showing recombined Td-Tomato$^+$ aNSCs from *Dicer* WT, *Dicer* HT, and *Dicer* cKO mice after 6 DIV with growth factors titration expressing DCX.

(C) Percentage of Td-Tomato$^+$ cells expressing DCX.

(D) Representative micrographs showing dendritic morphology of immature newly formed neurons expressing DCX.

Data are expressed as mean ± SEM, n = 3 independent experiments containing three replicates. One-way ANOVA Bonferroni as post hoc: *p < 0.05, ***p < 0.001. Scale bars, 50 μm.

(Figures S5C and S5D; Schouten et al., 2012), thus supporting the validity of our approach.

We hypothesized that miRNAs, whose expression is associated with early steps of neuronal fate choice, might rescue a DICER-dependent impairment on neurogenesis. We focused on a group of 11 miRNAs that showed a preferential enrichment (fold change log >2) and high levels of expression (<25 Ct values) during early neuronal differentiation (7 DIV): miR-376b-3p, 139-5p, 218-5p, 411-5p, 127-3p, 134-5p, 370-3p, 135a-5p, 382-5p, 708-5p, and 124-3p (Figure 5B, higher magnification; Figures 5C and S5E). To validate these miRNAs in vivo, we performed qRT-PCR analysis of total RNA from Tomato$^+$ cells that were FACS sorted 2 months after split-Cre infection of adult WT or *Dicer* cKO mice. We could detect most of these miRNAs in Tomato$^+$ WT cells as well as their significant reduction in *Dicer* cKO (Figure 5D). Next, we transfected in vitro WT and *Dicer* cKO aNSCs with control miRNAs, or *Dicer* cKO cells with a pool containing the 11 miRNAs (here referred as "total pool"). Six days after transfection, we found that the total pool, but not control miRNAs, rescued DICER-dependent impairment of neurogenesis to WT levels, as indicated by the expression of neuronal markers DCX (Figures 6A and 6B, p = 0.012; Figure 6E for mRNA quantification, p = 0.03) and MAP2 (Figures 6A and 6B, p = 0.0001). Moreover, we found a concomitant decrease in astrocytic differentiation from *Dicer* cKO aNSCs 6 days after transfection with the total pool, as revealed by a reduced expression of S100b (Figures 6A and 6B, p = 0.003) and *GFAP* mRNA (Figure 6E, p = 0.0019), indicating that these miRNAs were sufficient to control the switch between neuronal and astrocyte fates. Remarkably, when administered individually, or in subpools (chosen by the number of shared predicted targets involved in astrogliogenesis or neurogenesis, Table S2 and see below), we did not rescue neurogenesis impairment in *Dicer* cKO aNSCs (Figures 6C, 6E, and

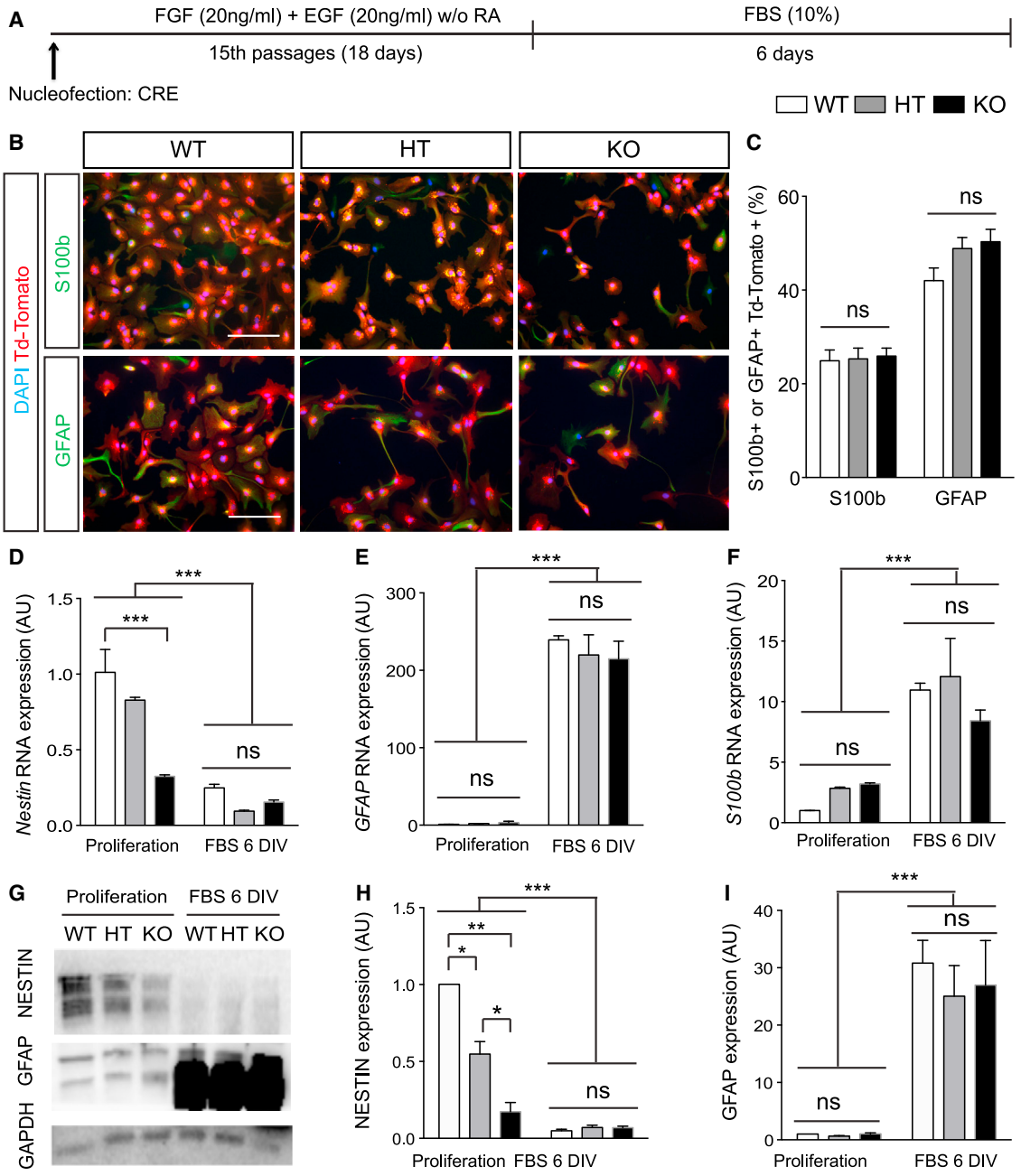

Figure 4. Loss of *Dicer*-Dependent miRNAs Does Not Affect Astrogliogenesis of aNSCs In Vitro

(A) Schematic representation of the protocol and experiment.

(B) Representative micrographs showing recombined Td-Tomato$^+$ aNSCs from *Dicer* WT, *Dicer* HT, and *Dicer* cKO mice after 6 DIV with 10% fetal bovine serum expressing S100b (upper panels) and GFAP (bottom panels).

(C) Percentage of Td-Tomato$^+$ cells expressing astrocyte markers (GFAP and S100b).

(D–F) Relative *Nestin* (D), *GFAP* (E), and *S100b* (F) mRNA quantification with qRT-PCR.

(G–I) Protein quantification of NESTIN (H) and GFAP (I).

Data are expressed as mean ± SEM, n = 3 independent experiments containing three replicates. One-way ANOVA Bonferroni as post hoc: *p < 0.05, **p < 0.01, ***p < 0.001. Scale bar, 50 μm.

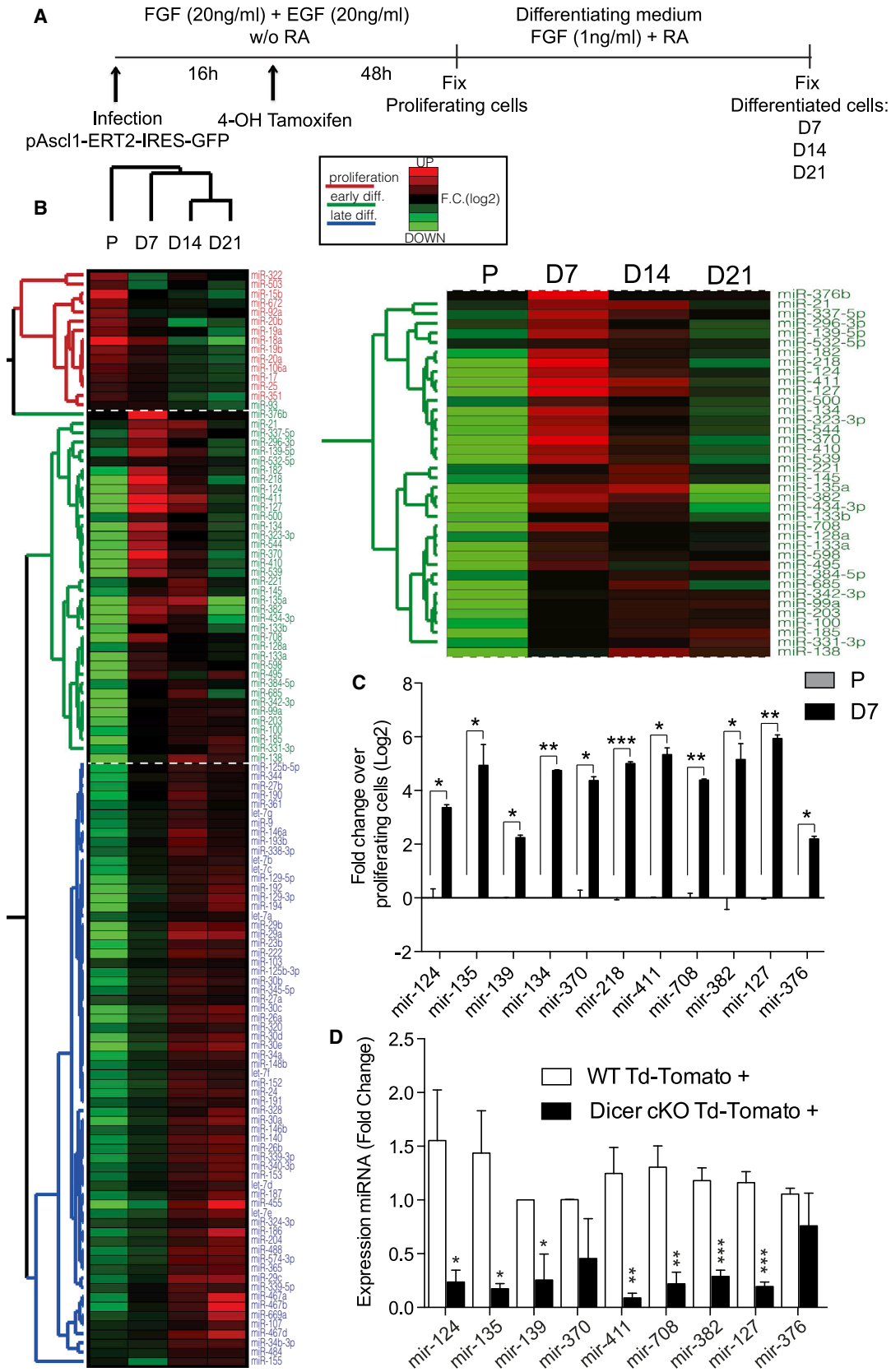

(legend on next page)

S6A). To further trim down the pool, we tested the withdrawal of individual miRNAs from the total pool in *Dicer* cKO aNSCs and found that none of them rescued neurogenesis impairment (Figure 6D). These experiments indicate that all of the 11 miRNAs are sufficient to rescue neuronal commitment in miRNA-depleted aNSCs.

To further ascertain whether these miRNAs are required, we conducted the opposite experiment by transfecting 11 miRNA inhibitors into WT aNSCs. We found a significant reduction in DCX^+ cells (Figures 7A and 7B, $p = 0.003$) and $MAP2^+$ cells (Figures 7A and 7B, $p = 0.0025$), but an increase in $S100b^+$ cells (Figures 7A and 7B, $p = 0.05$) compared with control WT cells. Taken together, these results demonstrate that 11 miRNAs are sufficient and required to sustain neuronal fate determination in hippocampal aNSCs, at the expense of astrogliogenesis, presumably through a synergic action.

Dissecting Pathways and Potential Targets Modulated by the 11 miRNAs in aNSCs

We hypothesized that the 11 miRNAs might synergize to simultaneously suppress pro-gliogenic and anti-neurogenic target genes. Consistently with this hypothesis, upon transfection of total miRNA pool (but not subpools), we found a significant reduction of the expression of negative regulators of neuronal differentiation, such as *SP1* ($p = 0.048$), or astrocyte differentiation such as *Tgfbr1* ($p = 0.0002$) (Figure S6B).

To further dissect potential targets and pathways modulated by the 11 miRNAs in aNSCs, we performed shotgun proteomics analysis in WT aNSCs transfected with the 11 miRNA inhibitors or control RNA and cultured them for 6 days in differentiating conditions. As expected, upon inhibition of 11 miRNAs we observed more upregulated proteins (>1.5-fold = 419; Figure 7C) than downregulated (<0.5-fold = 63; Figure 7C), compared with control inhibitors. Of interest, proteins dysregulated upon miRNA inhibition in aNSCs were enriched for metabolism (gene ontology [GO]: 44237; 59.8%, p = 2.5e-4) or cell cycle (GO: 7049; 16%, p=1.5e-5) processes, several of them, such as DRP2 (4.1 ± 0.5), NVL (1.53 ± 0.17), CNOT4 (12.66 ± 0.00), PTBP1 (1.63 ± 0.6), TLE1 (1.83 ± 0.6), and SFXN5 (1.64 ± 0.42) being highly expressed in astrocytes (Cahoy et al., 2008; Zhang et al., 2014) and predicted to be targeted by at least one of the 11 miRNA subjects of our study.

Next, we performed an in silico analysis to identify potential targets for the 11 miRNAs (Tables S1 and S2). We used miRWalk 2.0 with highly restrictive parameters, and found that a substantial fraction of the predicted targets (37%, i.e., 1,817 out of 4,929) were shared by at least two of the 11 miRNAs (Table S1) and had previously been shown to be expressed in developing astrocytes or neurons (Cahoy et al., 2008) (Figure S7).

To provide a molecular mechanism supporting the idea that synergic action of the 11 miRNAs is both necessary and sufficient to sustain adult neurogenesis, we compared the dysregulated proteins upon miRNA inhibition (Figure 7C) with the predicted targets (Table S1) and found 26 proteins of interest (Figure 7D). Remarkably, none of them was a predicted target of all miRNAs. Instead, they were predicted targets of different combinations of the selected miRNAs (Figure 7E). Moreover, based on analyses with DAVID (Jiao et al., 2012) or Reactome (Fabregat et al., 2016) software, we did not find any pathway that was shared between the 26 candidates. In contrast, GO analysis revealed that the 26 proteins shared similar biological processes (Figure 7F), such as nervous system development (GO: 7399; 30%, p = 0.011), neurogenesis (GO: 22008; 27%, p = 0.011), and neuron differentiation (GO: 30182; 24%, p = 0.023).

These results suggested that the 11 miRNAs cooperate by acting upon several targets within different pathways in parallel to determine adult neurogenesis.

DISCUSSION

Our study demonstrates that a set of 11 miRNAs (of which nine were not previously characterized in adult neurogenesis) is essential for neurogenic lineage fate determination of aNSCs in the adult hippocampus, and does so at the expense of astrogliogenesis. Remarkably, these miRNAs could rescue impaired neurogenesis in *Dicer* cKO aNSCs to WT levels only when administered as a pool, not individually. Thus our study provides evidence for the emerging

Figure 5. Profiling of miRNA Expression during Neuronal Differentiation of aNSCs In Vitro

(A) Schematic representation of the neuronal differentiation protocol with inducible retrovirus expressing ASCL1 (*Ascl1-ERT2-IRES-GFP*) and the experiment. Cells were collected during proliferation (P) or differentiation after 7 (D7), 14 (D14), and 21 (D21) DIV.

(B) Heatmap representing the set of miRNAs dynamically regulated upon neuronal differentiation at 7, 14, and 21 DIV. Red indicates high expression and green, low expression.

(C) Fold change of selected miRNAs during differentiation over proliferating cells.

(D) Fold change expression of miRNAs in vivo in FACS-sorted Td-$Tomato^+$ cells from ten adult *Dicer* WT and ten *Dicer* cKO mice 2 months after split-Cre recombinase virus injection into the DG. n = 3 independent experiments containing three replicates.

Data are expressed as mean ± SEM. Paired t test: *p < 0.05, **p < 0.01, ***p < 0.001.

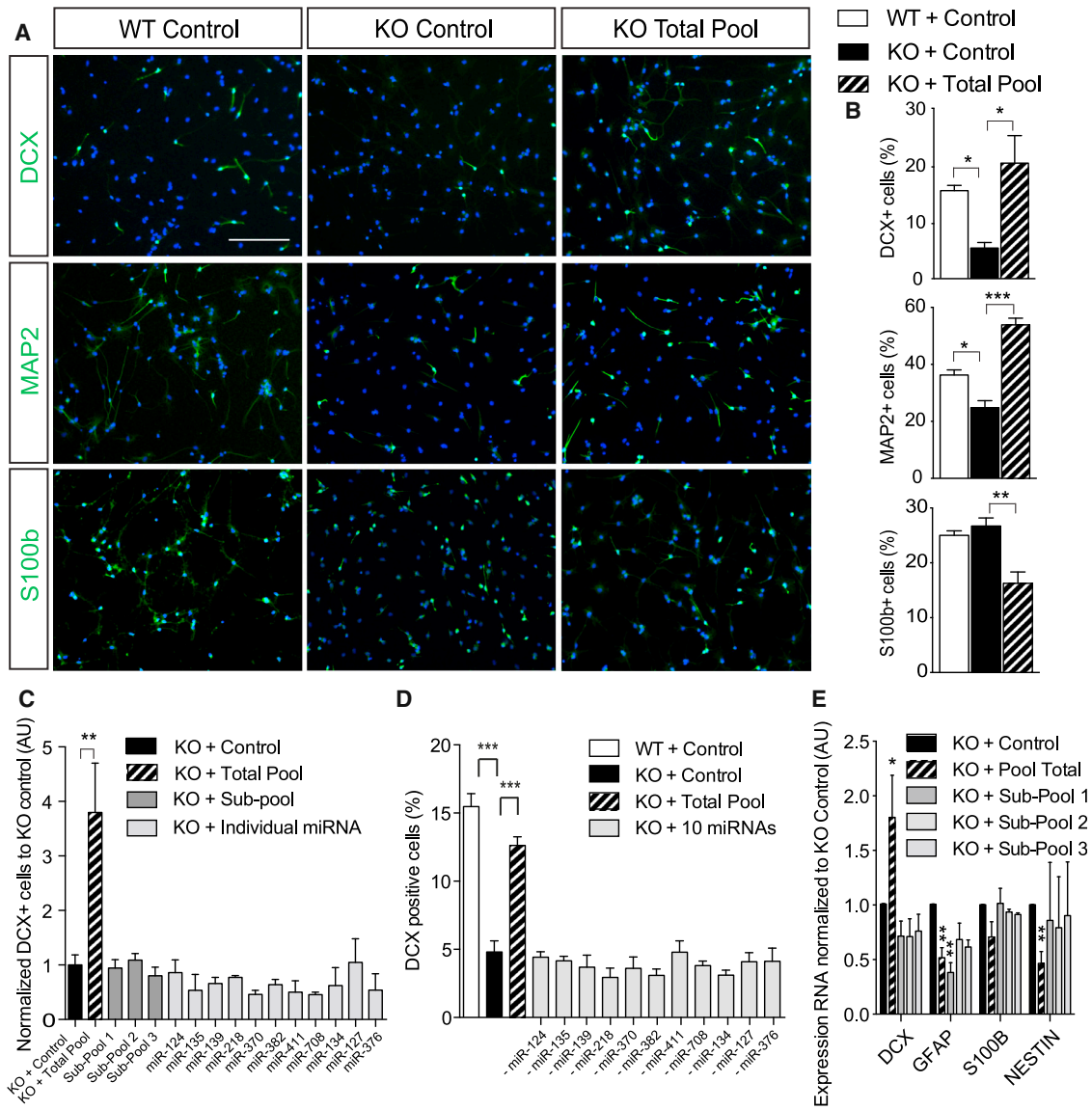

Figure 6. A Pool of 11 miRNAs Synergistically Rescues *Dicer* cKO Impairment of Adult Neurogenesis, at the Expense of Astrogliogenesis, In Vitro

(A) Representative micrographs showing aNSCs from *Dicer* WT and *Dicer* cKO mice transfected with 250 nM scrambled RNA or total pool (25 nM of each miRNA) after 6 DIV of growth factors withdrawal expressing DCX (upper panel), MAP2 (middle panel), and S100b (bottom panel). Scale bar, 50 μm.

(B) Percentage of DCX-, MAP2-, and S100b-positive aNSCs with respect to DAPI in WT and KO aNSCs transfected with scrambled RNA or total pool.

(C) Proportion of KO aNSCs expressing DCX upon transfection of 250 nM subpool 1 (mir-124-3p + mir-135a-5p), subpool 2 (mir-139-5p + mir-218-5p + mir-411-5p + mir-134-5p + mir-370-3p + mir-382-5p + mir-708-5p), subpool 3 (mir-127-3p + miR-376b-3p), or each miRNA alone with respect to KO control.

(D) Percentage of DCX-positive aNSCs with respect to DAPI after 6 DIV from WT or KO mice transfected with scrambled RNA, total pool, or a pool with ten miRNAs by the withdrawal of individual miRNAs.

(E) mRNA quantification with qRT-PCR from recombined KO aNSCs after 6 DIV.

Data are expressed as mean ± SEM, n ≥ 3 independent experiments containing three replicates. One-way ANOVA with Bonferroni as post hoc test: *p < 0.05, **p < 0.01, ***p < 0.001.

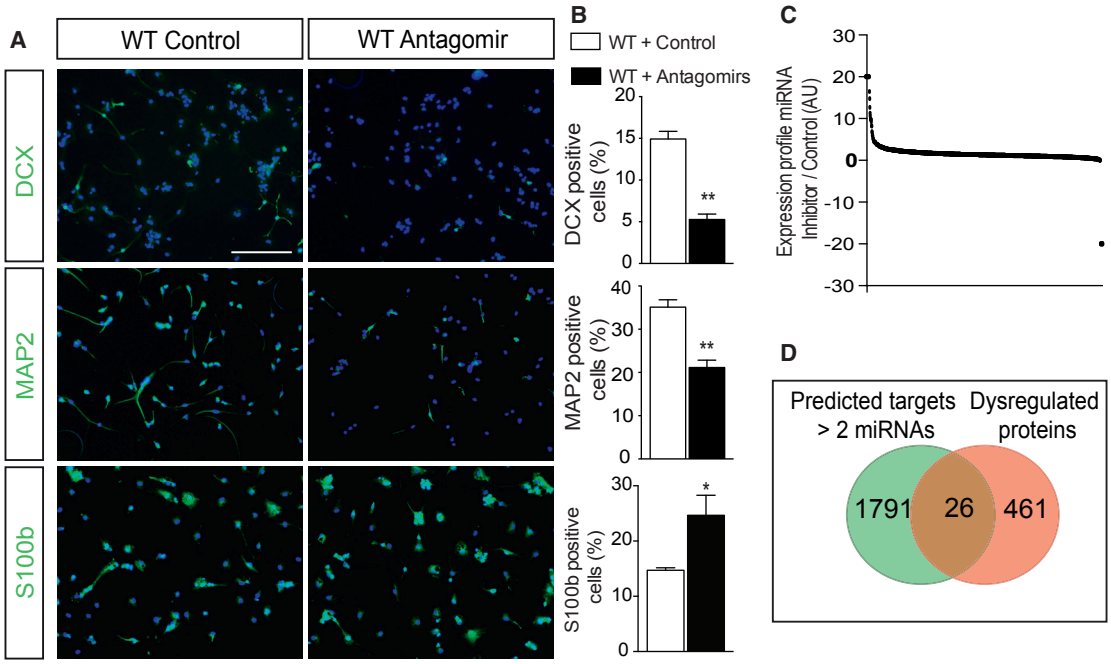

E

Fold change	ID	predicted to be targeted by miRNA
A.C	DRD5	miR-134-5p, miR-370-3p
12,663 +/-0,00	CNOT4	miR-124-3p, miR-376b-3p
4,104 +/-0,5	DRP2	miR-124-3p, miR-139-5p, miR-708-5p
3,886 +/-3,67	RC3H2	miR-139-5p, miR-218-5p, miR-708-5p
3,745 +/-4,25	LENG8	miR-370-3p, miR-708-5p
3,298 +/-1,72	PPIF	miR-124-3p, miR-370-3p
2,724 +/-3,27	LYZ1	miR-135a-5p, miR-139-5p
2,481 +/-1,94	RASEF	miR-124-3p, miR-382-5p
2,452 +/-1,20	VAT1	miR-124-3p, miR-218-5p
2,187 +/-0,89	LRP12	miR-370-3p, miR-382-5p, miR-708-5p
2,141 +/-1,74	ADCY1	miR-124-3p, miR-135a-5p, miR-139-5p, miR-218-5p, miR-370-3p, miR-382-5p
1,971 +/-2,17	ROCK2	miR-124-3p, miR-135a-5p, miR-411-5p
1,838 +/-0,79	TAOK1	miR-139-5p, miR-218-5p, miR-370-3p, miR-708-5p
1,796 +/-2,06	PARD3	miR-135a-5p, miR-134-5p, miR-370-3p
1,696 +/-1,47	UNC5D	miR-134-5p, miR-708-5p
1,651 +/-1,7	MKS1	miR-370-3p, miR-376b-3p
1,639 +/-0,42	SFXN5	miR-139-5p, miR-370-3p
1,587 +/-0,67	CENPW	miR-411-5p, miR-376b-3p
1,587 +/-0,71	BICD2	miR-124-3p, miR-370-3p
1,573 +/-0,78	TMOD1	miR-124-3p, miR-135a-5p
1,561 +/-0,74	AP5Z1	miR-370-3p, miR-382-5p
1,542 +/-0,72	FBXW8	miR-139-5p, miR-708-5p
1,534 +/-0,17	NVL	miR-382-5p, miR-411-5p
1,499 +/-1,20	FMR1	miR-124-3p, miR-134-5p, miR-139-5p
0,382 +/-0,21	UBN2	miR-124-3p miR-139-5p, miR-218-5p, miR-370-3p, miR-708-5p
A.I	PXDC1	miR-370-3p, miR-411-5p

F

Term	P value
GO:0071840~cellular component organization or biogenesis	0.0028
GO:0032989~cellular component morphogenesis	0.0049
GO:0016043~cellular component organization	0.0077
GO:0048666~neuron development	0.0091
GO:0022008~neurogenesis	0.011
GO:0007399~nervous system development	0.011
GO:0000904~cell morphogenesis involved in differentiation	0.015
GO:0006996~organelle organization	0.016
GO:0048858~cell projection morphogenesis	0.017
GO:0000902~cell morphogenesis	0.017
GO:0032990~cell part morphogenesis	0.018
GO:0048468~cell development	0.018
GO:0030182~neuron differentiation	0.023
GO:0030030~cell projection organization	0.024
GO:0031175~neuron projection development	0.024
GO:1900542~regulation of purine nucleotide metabolic process	0.026
GO:1902589~single-organism organelle organization	0.026
GO:0048667~cell morphogenesis involved in neuron differentiation	0.026
GO:0006140~regulation of nucleotide metabolic process	0.027
GO:0048812~neuron projection morphogenesis	0.032
GO:0045936~negative regulation of phosphate metabolic process	0.034
GO:0010563~negative regulation of phosphorus metabolic process	0.034
GO:0016358~dendrite development	0.035
GO:0048699~generation of neurons	0.035
GO:0070830~bicellular tight junction assembly	0.035
GO:0002064~epithelial cell development	0.035
GO:0045762~positive regulation of adenylate cyclase activity	0.040
GO:0009653~anatomical structure morphogenesis	0.042
GO:0051129~negative regulation of cellular component organization	0.044
GO:0043297~apical junction assembly	0.045

Figure 7. Convergence of the 11 miRNAs on Neurogenesis-Related Biological Processes

(A) Representative micrographs showing aNSCs from *Dicer* WT mice transfected with 250 nM scrambled RNA or a pool of miRNA inhibitors (antagomir) (25 nM of each miRNA inhibitor) after 6 DIV of growth factor withdrawal expressing DCX (upper panel), MAP2 (middle panel), and S100b (bottom panel).

(B) Percentage of DCX-, MAP2-, and S100b-positive aNSCs with respect to DAPI in WT aNSCs transfected with scrambled RNA or pool inhibitor.

(C) Expression proteomics profile of miRNA inhibitor with respect to control group at 6 DIV.

(D) Venn diagram showing the putative predicted targets by at least two miRNAs from the in silico analysis that are significantly dysregulated in the proteomics analysis upon miRNA inhibitor administration.

(E) Dysregulated proteins that are putatively targeted by at least two miRNAs. Fold change and SD for WT aNSCs transfected with a pool of inhibitors versus control RNA for each protein expression and predicted targeting miRNAs are shown. A.C, absent in control samples; A.I, absent in miRNA inhibitor samples.

(F) Gene ontology (GO) analysis significantly represented for the 26 predicted common targets dysregulated upon miRNA inhibition.

Data are expressed as mean ± SEM, n = 3 independent experiments containing three replicates. Unpaired t test: *p < 0.05, **p < 0.01. Scale bar, 50 μm.

notion of miRNA "convergence" (or "cooperativity") that, by synergistic enforcement of gene-regulatory networks, allows the acquisition of neurogenic fate programming in aNSCs.

Adult neurogenesis is a highly conserved process among vertebrates (Gage and Temple, 2013). However, the mechanisms underlying the control of a proper acquisition of the neurogenic versus astrogliogenic fate remains a fundamental question in the field (Bonaguidi et al., 2012; Kempermann, 2011). Here, by targeting bona fide type I aNSCs in vivo and in vitro, we show that loss of DICER-dependent miRNAs in aNSCs impaired neurogenesis but not astrogliogenesis. Thus our results uncover miRNAs as a regulatory level necessary to sustain neurogenic lineage and prevent astrogliogenesis in the adult hippocampal niche. This evidence reinforces the emerging idea that multiple layers of control are required to allow adult neurogenesis to occur properly. This has recently been demonstrated for other epigenetic mechanisms in a similar way (Lv et al., 2013; Noguchi et al., 2015).

An interesting question is why, given these results, DICER/miRNA-depleted aNSCs can still undergo astrocytic differentiation at all? Based on our results, and given the proposed glial nature of aNSCs (Brunne et al., 2010; Kriegstein and Alvarez-Buylla, 2009; Nicola et al., 2015), which share common molecular pathways with non-neurogenic astrocytes (Beckervordersandforth et al., 2014; Buffo et al., 2008; Coskun et al., 2008), we postulate that the gliogenic program in aNSCs might represent rather a "default" developmental path than a fate change, and thus be less dependent on miRNAs (Encinas et al., 2011). Despite we cannot rule out that "immature or intermediate" astrocytes are generated by *Dicer*-depleted aNSCs in vivo, these newborn cells (as revealed by Td-Tomato and BrdU) were also positive for different astrocytic markers, such as S100b (Figures 1E and 1H) and GS (Figures S1B and S1C) 2 months after *Dicer* deletion. Moreover, since upon *Dicer* ablation we did not find increased expression of progenitor markers such as Nestin or SOX2 (Figures S1B and S1C), we postulate that these cells might be bona fide astrocytes, rather than aNSCs remaining in undifferentiated (or returning) or quiescent state. Another possibility is that miRNA-depleted newborn neurons could be more susceptible to apoptosis compared with astrocytes. However, differentiating aNSC *Dicer* HT (Figure 2) were not more susceptible than WT cells to apoptosis (Figure S4), but still gave rise to fewer neurons (Figure 3). This suggests that miRNA loss in aNSCs can affect the switch toward neurogenesis independently from cell death. Finally, it is still possible that different subtypes of neural and glial progenitor cells exist in the adult hippocampal niche that responds differently to miRNA depletion; hence in the absence of Dicer/miRNAs neurogenesis fails while astrogliogenesis is proportionally increased. This scenario would be consistent with the known heterogeneity of aNSCs (Shin et al., 2015). However, we can still conclude that loss of *Dicer* and DICER-dependent miRNAs does not impair astrogliogenesis in the adult hippocampal stem cell niche.

Although, due to limitations of the current tools and technical challenges, we could not perform direct manipulation of the 11 miRNAs to rescue/inhibit neurogenesis in vivo, we demonstrated that most of these miRNAs are expressed in adult-born hippocampal neurons, and consequently depleted upon the loss of *Dicer* in vivo. Moreover, our in vitro experiments identify that all of the 11 miRNAs are sufficient to rescue DICER-dependent impairment of neurogenesis (Figure 6) and are required to sustain neurogenesis in WT aNSCs (Figure 7). Together, these results strongly indicate that miRNAs, rather than other additional DICER functions, determine neuronal fate of aNSCs. In perspective, our approach might be a useful paradigm to functionally investigate other miRNAs and targets. For example, 6 of the 11 miRNAs of our study are encoded by the *Dlk1-Dio3* imprinted genomic region, containing the mirG locus that is highly enriched with miRNAs and deregulated in neurodevelopmental disorders and brain tumors (Gardiner et al., 2012; Henriksen et al., 2014). This locus also encodes miR-134, which is important for neuronal synaptogenesis and plasticity (Schratt et al., 2006).

The proposed synergy of miRNA actions refers to the "convergence" or "cooperativity" of miRNAs as a rapidly emerging theme in neurobiology, and has recently been proposed for embryonic neurogenesis (Barca-Mayo and De Pietri Tonelli, 2014), the adult SVZ (Santos et al., 2016), and apoptosis in the adult DG (Schouten et al., 2015). Consistent with this idea, we identified 26 putative targets of the 11 miRNAs that did not share immediate involvement in any pathway, but synergistically regulate biological processes such as neurogenesis, nervous system development, and neuronal differentiation. These results are consistent with our model whereby miRNAs "converge on function" (Barca-Mayo and De Pietri Tonelli, 2014). Given that each of the 11 miRNAs individually did not significantly induce neurogenesis, the synergic action on several targets from different pathways in parallel might compensate for the mild degree of miRNA-dependent regulation of individual mRNA targets. Further studies will be essential to experimentally validate the miRNAs and targets that are, in combination, key in regulating aNSCs neurogenesis.

Finally, the identification of a set of miRNAs that determines neuronal fate of aNSCs raises interesting perspectives with regard to age-dependent loss of hippocampal neurogenesis (Marlatt and Lucassen, 2010) or the generation of undesirable cells upon insults or cell transplantation (Dibajnia and Morshead, 2013; Doetsch et al., 2002; Shimada et al., 2012; Sierra et al., 2015). Perhaps

administration of the miRNAs that were the subject of this study will increase our repertoire of approaches to sustain neurogenesis in the aging brain, or to improve efficiency of NSC-based regenerative therapies.

EXPERIMENTAL PROCEDURES

Animals

Mice were housed under standard laboratory conditions at Istituto Italiano di Tecnologia (IIT). All experiments and procedures were approved by the Italian authorities (permit nos. 056/2013 and 214/2015-PR) and were conducted in accordance with the Guide for the Care and Use of Laboratory Animals of the European Community Council Directives. *Dicer*$^{flox/flox}$ mice (Murchison et al., 2005) were crossed with *Td-Tomato*$^{flox/wt}$ knockin reporter mice (Jackson Laboratory stock number 007908; Madisen et al., 2010). *Dicer*$^{wt/wt}$ *Td-Tomato*$^{flox/wt}$ (*Dicer* WT), *Dicer*$^{flox/wt}$ *Td-Tomato*$^{flox/wt}$ (*Dicer* HT), and *Dicer*$^{flox/flox}$ *Td-Tomato*$^{flox/wt}$ (*Dicer* cKO) were used for experiments.

aNSC Preparation, Culture Conditions, and miRNA Administration

Hippocampal NSCs were prepared and expanded as described previously (Babu et al., 2011; Walker and Kempermann, 2014). *Dicer* ablation was obtained in proliferating aNSCs by nucleofection (Amaxa, Lonza) of 5 μg of Cre recombinase-expressing vector under the control of constitutive cytomegalovirus enhancer/chicken β-actin (CAG) promoter (pCAGGS-CRE). Detailed cell-culture protocols are described in Supplemental Experimental Procedures. For miRNA administration, proliferating aNSCs were nucleofected (Amaxa, Lonza) with a pool of mimics or antagomirs at equimolar concentration to a final concentration 250 nM (Dharmacon, negative control, CN-001000-01-05); or with a mix of individual miRNA mimics each at 25 nM, plus negative control to a final concentration of 250 nM. Twenty-four hours after nucleofection, cells were plated in differentiation medium and harvested after 6 days.

Immunofluorescence

Immunofluorescence staining on brain slices was performed in one of every six sections of the hippocampus. A list of primary antibodies and detailed protocol are provided in Supplemental Experimental Procedures. Images were obtained with the Confocal A1 Nikon Inverted SFC with 40× objective. Quantification and analysis in the DG was performed using NIS-Elements software (Nikon). Immunofluorescence on cell cultures was performed as previously described (Babu et al., 2011). Images were obtained using the microscope Nikon Eclipse at 20× or 40× magnification, and cell-counter plugin in ImageJ software (Macbiophotonics) was used to keep track of counted cells.

RNA/Protein Extraction, Analysis, and Proteomics

For RNA extraction and cDNA preparation, six to ten mice (each Dicer genotype) were euthanized at the indicated time points. DG cells were dissociated with the Neural Tissue Dissociation Kit P (Miltenyi Biotec), and FACS-sorted cells were immediately processed for RNA extraction. Cre-nucleofected aNSCs in culture were harvested at the indicated time points. Total RNA was extracted with QIAzol protocol (Qiagen) and RNA purified with RNeasy Mini Kit, or miRNeasy Mini Kit (Qiagen) following the manufacturer's instructions. cDNA (for mRNAs) synthesis was obtained with ImProm-II reverse transcriptase (Promega); cDNA (from miRNA) was prepared with an miScript II RT kit using the HiSpec Buffer (Qiagen) according to the manufacturer's instructions. mRNA was quantified with a QuantiFast SYBR Green PCR Kit (Qiagen) on a ABI-7500 Real-Time PCR System (Applied Biosystems). Each sample was normalized to *GAPDH* or *Actin* levels. Specific primers used for gene expression analysis are listed in Supplemental Experimental Procedures. miRNAs were quantified with the Mouse Cell Differentiation & Development miScript miRNA PCR Array (Qiagen) and miScript SYBR Green PCR kit (Qiagen) following the manufacturer's recommendations on an ABI-7500 Real-Time PCR System (Applied Biosystems) or with TaqMan Array Rodent MicroRNA A Cards Set v3.0 (Thermo Fisher) following the manufacturer's recommendations with a ViiA 7 Real-Time PCR system (Thermo Fisher), for which original Ct values are available on request. For western blotting, proteins were extracted from aNSCs by RIPA buffer containing protease inhibitors (Complete mini EDTA-free, Roche), separated by SDS-PAGE on a 10% Tris gradient gel and transferred to a nitrocellulose membrane (Bio-Rad). Membranes were probed overnight using primary antibodies: rabbit GFAP (1:5,000; catalog no. Z-0334, Dako), rat anti-NESTIN (1:1,000; 556309, BD-Pharmingen), rabbit GAPDH (1:4500; AM4300, Applied Biosystems), and secondary horseradish peroxidase-conjugated antibodies (1:2,500; anti-rabbit immunoglobulin G [IgG], A16074, Life Technologies; anti-rat IgG, 31470, Thermo Fisher). Bands were detected by ECL (Millipore) using ImageQuant LAS 4000 Mini (GE Healthcare) and quantified using ImageJ software.

For proteomics, aNSCs (three independent experiments) were lysed with RIPA buffer and 60 μg of proteins was collected from all the samples to isobarically label them using TMT Sixplex kits (Thermo Fisher Scientific). Protein pools were processed for liquid chromatography-tandem mass spectrometry analysis (see Supplemental Experimental Procedures).

Statistical Analysis

Data are presented as mean ± SEM and were analyzed using Prism 6 (GraphPad). Statistical significance was assessed with a two-tailed unpaired t test for two experimental groups. For experiments with three or more groups, one-way ANOVA with Bonferroni's multiple comparison test as post hoc was used. Results were considered significant when $p < 0.05$.

SUPPLEMENTAL INFORMATION

Supplemental Information includes Supplemental Experimental Procedures, seven figures, and three tables and can be found with this article online at http://dx.doi.org/10.1016/j.stemcr.2017.02.012.

AUTHOR CONTRIBUTIONS

M.P.E. performed all experiments and analyses, and co-wrote the manuscript. E.d.L. performed some in vitro experiments and analysis. Initial preparation of in vitro hippocampal aNSC cultures was

performed in the G.K. laboratory under the supervision of K.F. M.J.M. performed analysis of miRNA qRT-PCR in the F.N. laboratory, who supervised this part of the work. R.B. produced initial stocks and helped to set up split-Cre virus. A.A. performed and analyzed the proteomics expression experiments. D.D.P.T conceived and coordinated the project and co-wrote the manuscript. All authors approved the final version of the manuscript.

ACKNOWLEDGMENTS

We thank Dr. G. Hannon (Cold Spring Harbor Laboratory, USA) for kindly providing *Dicer*-Flox mouse line; Dr. S. Jessberger (University of Zurich, Switzerland) for Ascl1-ERT2-IRES-GFP viral construct; and Drs M. Götz and J. Ninkovic (Helmholtz Zentrum, München, Germany) for the split-Cre viral constructs. We thank Drs. P. Oloth (DZNE), T. Walker (CRTD), A. Simi, and A Contestabile (IIT) for advice on aNSC preparation and differentiation. We thank R. Pelizzoli and IIT-NBT technical staff (M. Pesce, F. Succol, and M. Nanni) for excellent help. We also thank the Animal Facility of IIT Genoa (F. Piccardi; D. Cantatore; R. Navone, and M. Morini) for assistance in animal experiments. D.D.P.T. was supported by intramural funds of Fondazione Istituto Italiano di Tecnologia. This research was supported by intramural funds of Fondazione Istituto Italiano di Tecnologia and by Fondazione Cariplo grant no. 2015-0590 to D.D.P.T. and F.N.

Received: July 12, 2016
Revised: February 10, 2017
Accepted: February 10, 2017
Published: March 16, 2017

REFERENCES

Agarwal, V., Bell, G.W., Nam, J.-W., and Bartel, D.P. (2015). Predicting effective microRNA target sites in mammalian mRNAs. Elife *4*. http://dx.doi.org/10.7554/eLife.05005.

Aksoy-Aksel, A., Zampa, F., and Schratt, G. (2014). MicroRNAs and synaptic plasticity—a mutual relationship. Philos. Trans. R. Soc. Lond. B. Biol. Sci. *369*. http://dx.doi.org/10.1098/rstb.2013.0515.

Andersson, T., Rahman, S., Sansom, S.N., Alsiö, J.M., Kaneda, M., Smith, J., O'Carroll, D., Tarakhovsky, A., and Livesey, F.J. (2010). Reversible block of mouse neural stem cell differentiation in the absence of dicer and microRNAs. PLoS One *5*, e13453.

Babu, H., Claasen, J.-H., Kannan, S., Rünker, A.E., Palmer, T., and Kempermann, G. (2011). A protocol for isolation and enriched monolayer cultivation of neural precursor cells from mouse dentate gyrus. Front. Neurosci. *5*, 89.

Barca-Mayo, O., and De Pietri Tonelli, D. (2014). Convergent microRNA actions coordinate neocortical development. Cell. Mol. Life Sci. *71*, 2975–2995.

Beckervordersandforth, R., Deshpande, A., Schäffner, I., Huttner, H.B., Lepier, A., Lie, D.C., and Götz, M. (2014). In vivo targeting of adult neural stem cells in the dentate gyrus by a split-cre approach. Stem Cell Rep. *2*, 153–162.

Beckervordersandforth, R., Zhang, C.-L., and Lie, D.C. (2015). Transcription-factor-dependent control of adult hippocampal neurogenesis. Cold Spring Harb. Perspect. Biol. *7*, a018879.

Bonaguidi, M.A., Song, J., Ming, G., and Song, H. (2012). A unifying hypothesis on mammalian neural stem cell properties in the adult hippocampus. Curr. Opin. Neurobiol. *22*, 754–761.

Bond, A.M., Ming, G., and Song, H. (2015). Adult mammalian neural stem cells and neurogenesis: five decades later. Cell Stem Cell *17*, 385–395.

Braun, S.M.G., Machado, R.A.C., and Jessberger, S. (2013). Temporal control of retroviral transgene expression in newborn cells in the adult brain. Stem Cell Rep. *1*, 114–122.

Brunne, B., Zhao, S., Derouiche, A., Herz, J., May, P., Frotscher, M., and Bock, H.H. (2010). Origin, maturation, and astroglial transformation of secondary radial glial cells in the developing dentate gyrus. Glia *58*, 1553–1569.

Buffo, A., Rite, I., Tripathi, P., Lepier, A., Colak, D., Horn, A.-P., Mori, T., and Götz, M. (2008). Origin and progeny of reactive gliosis: a source of multipotent cells in the injured brain. Proc. Natl. Acad. Sci. USA *105*, 3581–3586.

Cahoy, J.D., Emery, B., Kaushal, A., Foo, L.C., Zamanian, J.L., Christopherson, K.S., Xing, Y., Lubischer, J.L., Krieg, P.A., Krupenko, S.A., et al. (2008). A transcriptome database for astrocytes, neurons, and oligodendrocytes: a new resource for understanding brain development and function. J. Neurosci. *28*, 264–278.

Castel, S.E., and Martienssen, R.A. (2013). RNA interference in the nucleus: roles for small RNAs in transcription, epigenetics and beyond. Nat. Rev. Genet. *14*, 100–112.

Cernilogar, F.M., Onorati, M.C., Kothe, G.O., Burroughs, A.M., Parsi, K.M., Breiling, A., Lo Sardo, F., Saxena, A., Miyoshi, K., Siomi, H., et al. (2011). Chromatin-associated RNA interference components contribute to transcriptional regulation in Drosophila. Nature *480*, 391–395.

Cheng, L.-C., Pastrana, E., Tavazoie, M., and Doetsch, F. (2009). miR-124 regulates adult neurogenesis in the subventricular zone stem cell niche. Nat. Neurosci. *12*, 399–408.

Coskun, V., Wu, H., Blanchi, B., Tsao, S., Kim, K., Zhao, J., Biancotti, J.C., Hutnick, L., Krueger, R.C., Fan, G., et al. (2008). CD133+ neural stem cells in the ependyma of mammalian postnatal forebrain. Proc. Natl. Acad. Sci. USA *105*, 1026–1031.

De Pietri Tonelli, D., Pulvers, J.N., Haffner, C., Murchison, E.P., Hannon, G.J., and Huttner, W.B. (2008). miRNAs are essential for survival and differentiation of newborn neurons but not for expansion of neural progenitors during early neurogenesis in the mouse embryonic neocortex. Development *135*, 3911–3921.

Dibajnia, P., and Morshead, C.M. (2013). Role of neural precursor cells in promoting repair following stroke. Acta Pharmacol. Sin. *34*, 78–90.

Doetsch, F., Petreanu, L., Caille, I., Garcia-Verdugo, J.-M., and Alvarez-Buylla, A. (2002). EGF converts transit-amplifying neurogenic precursors in the adult brain into multipotent stem cells. Neuron *36*, 1021–1034.

Encinas, J.M., Michurina, T.V., Peunova, N., Park, J.-H., Tordo, J., Peterson, D.A., Fishell, G., Koulakov, A., and Enikolopov, G. (2011). Division-coupled astrocytic differentiation and age-related depletion of neural stem cells in the adult hippocampus. Cell Stem Cell *8*, 566–579.

Fabregat, A., Sidiropoulos, K., Garapati, P., Gillespie, M., Hausmann, K., Haw, R., Jassal, B., Jupe, S., Korninger, F., McKay, S., et al. (2016). The reactome pathway knowledge base. Nucleic Acids Res. *44*, D481–D487.

Friedman, R.C., Farh, K.K.-H., Burge, C.B., and Bartel, D.P. (2009). Most mammalian mRNAs are conserved targets of microRNAs. Genome Res. *19*, 92–105.

Gage, F.H., and Temple, S. (2013). Neural stem cells: generating and regenerating the brain. Neuron *80*, 588–601.

Gardiner, E., Beveridge, N.J., Wu, J.Q., Carr, V., Scott, R.J., Tooney, P.A., and Cairns, M.J. (2012). Imprinted DLK1-DIO3 region of 14q32 defines a schizophrenia-associated miRNA signature in peripheral blood mononuclear cells. Mol. Psychiatry *17*, 827–840.

Ha, M., and Kim, V.N. (2014). Regulation of microRNA biogenesis. Nat. Rev. Mol. Cell Biol. *15*, 509–524.

Henriksen, M., Johnsen, K.B., Olesen, P., Pilgaard, L., and Duroux, M. (2014). MicroRNA expression signatures and their correlation with clinicopathological features in glioblastoma multiforme. Neuromolecular Med. *16*, 565–577.

Huang, V., and Li, L.-C. (2014). Demystifying the nuclear function of Argonaute proteins. RNA Biol. *11*, 18–24.

Jiao, X., Sherman, B.T., Huang, D.W., Stephens, R., Baseler, M.W., Lane, H.C., and Lempicki, R.A. (2012). DAVID-WS: a stateful web service to facilitate gene/protein list analysis. Bioinformatics *28*, 1805–1806.

Kempermann, G. (2011). The pessimist's and optimist's views of adult neurogenesis. Cell *145*, 1009–1011.

Kempermann, G., Song, H., and Gage, F.H. (2015). Neurogenesis in the adult Hippocampus. Cold Spring Harb. Perspect. Med. *5*, a018812.

Konopka, W., Kiryk, A., Novak, M., Herwerth, M., Parkitna, J.R., Wawrzyniak, M., Kowarsch, A., Michaluk, P., Dzwonek, J., Arnsperger, T., et al. (2010). MicroRNA loss enhances learning and memory in mice. J. Neurosci. *30*, 14835–14842.

Kriegstein, A., and Alvarez-Buylla, A. (2009). The glial nature of embryonic and adult neural stem cells. Annu. Rev. Neurosci. *32*, 149–184.

Krol, J., Loedige, I., and Filipowicz, W. (2010). The widespread regulation of microRNA biogenesis, function and decay. Nat. Rev. Genet. *11*, 597–610.

Li, L.-C. (2014). Chromatin remodeling by the small RNA machinery in mammalian cells. Epigenetics *9*, 45–52.

Lim, L.P., Lau, N.C., Garrett-Engele, P., Grimson, A., Schelter, J.M., Castle, J., Bartel, D.P., Linsley, P.S., and Johnson, J.M. (2005). Microarray analysis shows that some microRNAs downregulate large numbers of target mRNAs. Nature *433*, 769–773.

Lv, J., Xin, Y., Zhou, W., and Qiu, Z. (2013). The epigenetic switches for neural development and psychiatric disorders. J. Genet. Genomics *40*, 339–346.

Madisen, L., Zwingman, T.A., Sunkin, S.M., Oh, S.W., Zariwala, H.A., Gu, H., Ng, L.L., Palmiter, R.D., Hawrylycz, M.J., Jones, A.R., et al. (2010). A robust and high-throughput Cre reporting and characterization system for the whole mouse brain. Nat. Neurosci. *13*, 133–140.

Magill, S.T., Cambronne, X.A., Luikart, B.W., Lioy, D.T., Leighton, B.H., Westbrook, G.L., Mandel, G., and Goodman, R.H. (2010). microRNA-132 regulates dendritic growth and arborization of newborn neurons in the adult hippocampus. Proc. Natl. Acad. Sci. USA *107*, 20382–20387.

Marlatt, M.W., and Lucassen, P.J. (2010). Neurogenesis and Alzheimer's disease: biology and pathophysiology in mice and men. Curr. Alzheimer Res. *7*, 113–125.

Murchison, E.P., Partridge, J.F., Tam, O.H., Cheloufi, S., and Hannon, G.J. (2005). Characterization of Dicer-deficient murine embryonic stem cells. Proc. Natl. Acad. Sci. USA *102*, 12135–12140.

Nicola, Z., Fabel, K., and Kempermann, G. (2015). Development of the adult neurogenic niche in the hippocampus of mice. Front. Neuroanat. *9*, 53.

Noguchi, H., Kimura, A., Murao, N., Matsuda, T., Namihira, M., and Nakashima, K. (2015). Expression of DNMT1 in neural stem/precursor cells is critical for survival of newly generated neurons in the adult hippocampus. Neurosci. Res. *95*, 1–11.

Pons-Espinal, M., de Lagran, M.M., and Dierssen, M. (2013). Functional implications of hippocampal adult neurogenesis in intellectual disabilities. Amino Acids *45*, 113–131.

Santos, M.C.T., Tegge, A.N., Correa, B.R., Mahesula, S., Kohnke, L.Q., Qiao, M., Ferreira, M.A.R., Kokovay, E., and Penalva, L.O.F. (2016). miR-124, -128, and -137 orchestrate neural differentiation by acting on overlapping gene sets containing a highly connected transcription factor network. Stem Cells *34*, 220–232.

Schmiedel, J.M., Klemm, S.L., Zheng, Y., Sahay, A., Blüthgen, N., Marks, D.S., and van Oudenaarden, A. (2015). Gene expression. MicroRNA control of protein expression noise. Science *348*, 128–132.

Schouten, M., Buijink, M.R., Lucassen, P.J., and Fitzsimons, C.P. (2012). New neurons in aging brains: molecular control by small non-coding RNAs. Front. Neurosci. *6*, 25.

Schouten, M., Fratantoni, S.A., Hubens, C.J., Piersma, S.R., Pham, T.V., Bielefeld, P., Voskuyl, R.A., Lucassen, P.J., Jimenez, C.R., and Fitzsimons, C.P. (2015). MicroRNA-124 and -137 cooperativity controls caspase-3 activity through BCL2L13 in hippocampal neural stem cells. Sci. Rep. *5*, 12448.

Schratt, G.M., Tuebing, F., Nigh, E.A., Kane, C.G., Sabatini, M.E., Kiebler, M., and Greenberg, M.E. (2006). A brain-specific microRNA regulates dendritic spine development. Nature *439*, 283–289.

Selbach, M., Schwanhäusser, B., Thierfelder, N., Fang, Z., Khanin, R., and Rajewsky, N. (2008). Widespread changes in protein synthesis induced by microRNAs. Nature *455*, 58–63.

Shimada, I.S., LeComte, M.D., Granger, J.C., Quinlan, N.J., and Spees, J.L. (2012). Self-renewal and differentiation of reactive astrocyte-derived neural stem/progenitor cells isolated from the cortical peri-infarct area after stroke. J. Neurosci. *32*, 7926–7940.

Shin, J., Berg, D.A., Zhu, Y., Shin, J.Y., Song, J., Bonaguidi, M.A., Enikolopov, G., Nauen, D.W., Christian, K.M., Ming, G., et al. (2015). Single-cell RNA-Seq with waterfall reveals molecular cascades underlying adult neurogenesis. Cell Stem Cell *17*, 360–372.

Siciliano, V., Garzilli, I., Fracassi, C., Criscuolo, S., Ventre, S., and di Bernardo, D. (2013). miRNAs confer phenotypic robustness to

gene networks by suppressing biological noise. Nat. Commun. *4*, 2364.

Sierra, A., Martín-Suárez, S., Valcárcel-Martín, R., Pascual-Brazo, J., Aelvoet, S.-A., Abiega, O., Deudero, J.J., Brewster, A.L., Bernales, I., Anderson, A.E., et al. (2015). Neuronal hyperactivity accelerates depletion of neural stem cells and impairs hippocampal neurogenesis. Cell Stem Cell *16*, 488–503.

Smrt, R.D., Szulwach, K.E., Pfeiffer, R.L., Li, X., Guo, W., Pathania, M., Teng, Z.-Q., Luo, Y., Peng, J., Bordey, A., et al. (2010). MicroRNA miR-137 regulates neuronal maturation by targeting ubiquitin ligase Mind Bomb-1. Stem Cells *28*, 1060–1070.

Walker, T.L., and Kempermann, G. (2014). One mouse, two cultures: isolation and culture of adult neural stem cells from the two neurogenic zones of individual mice. J. Vis. Exp., e51225.

Yang, J.-S., and Lai, E.C. (2011). Alternative miRNA biogenesis pathways and the interpretation of core miRNA pathway mutants. Mol. Cell *43*, 892–903.

Zhang, Y., Chen, K., Sloan, S.A., Bennett, M.L., Scholze, A.R., O'Keeffe, S., Phatnani, H.P., Guarnieri, P., Caneda, C., Ruderisch, N., et al. (2014). An RNA-sequencing transcriptome and splicing database of glia, neurons, and vascular cells of the cerebral cortex. J. Neurosci. *34*, 11929–11947.

Zhao, C., Sun, G., Li, S., and Shi, Y. (2009). A feedback regulatory loop involving microRNA-9 and nuclear receptor TLX in neural stem cell fate determination. Nat. Struct. Mol. Biol. *16*, 365–371.

Zhu, W., Yang, L., and Du, Z. (2011). MicroRNA regulation and tissue-specific protein interaction network. PLoS One *6*, e25394.

Stem Cell Reports, Volume *8*

Supplemental Information

Synergic Functions of miRNAs Determine Neuronal Fate of Adult Neural Stem Cells

Meritxell Pons-Espinal, Emanuela de Luca, Matteo Jacopo Marzi, Ruth Beckervordersandforth, Andrea Armirotti, Francesco Nicassio, Klaus Fabel, Gerd Kempermann, and Davide De Pietri Tonelli

SUPPLEMENTAL INFORMATION

Supplemental Figures and Figure Legends

Figure S1. Related to Figure 1 and Figure 2.

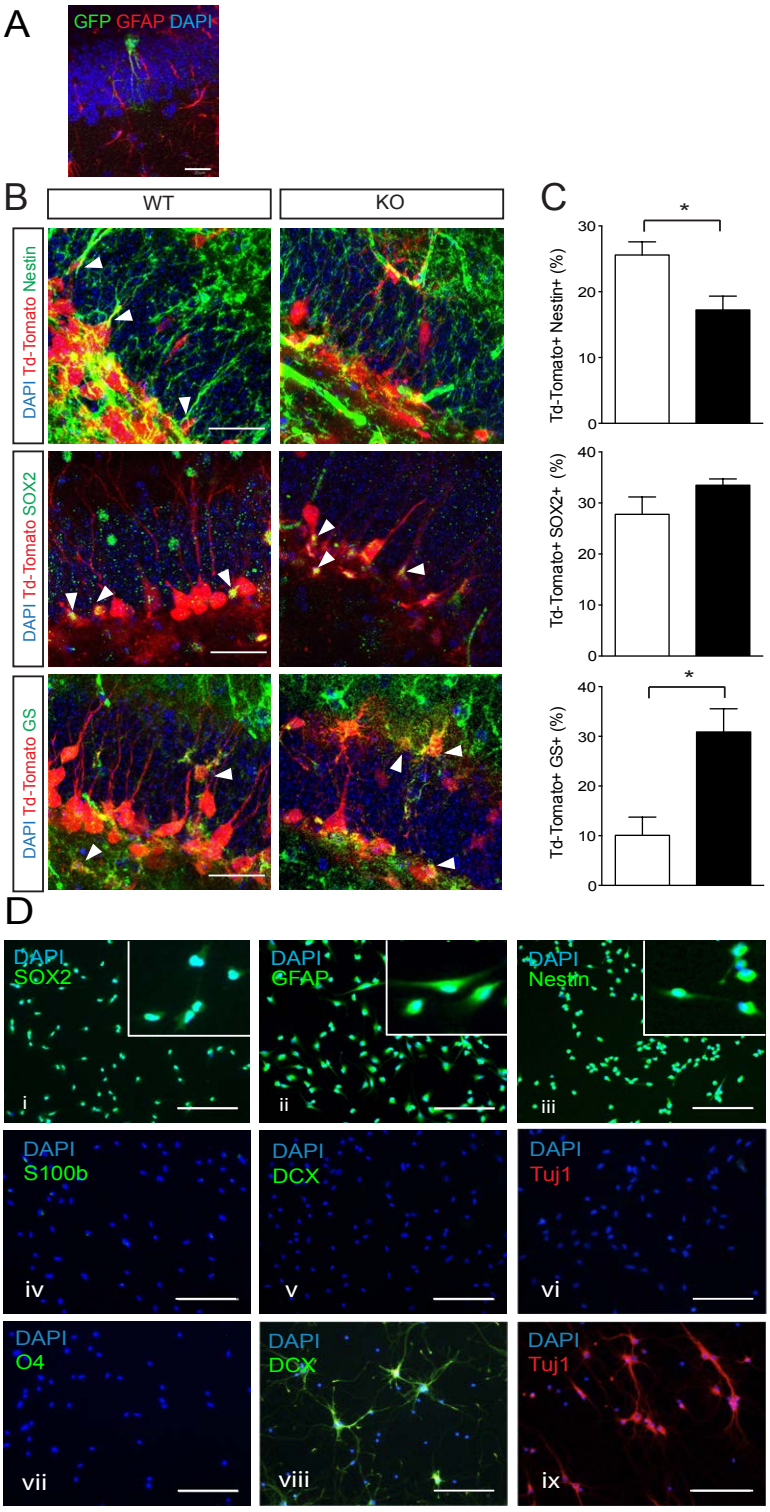

Figure S1. Characterization of adult neural stem cells subject of the study *in vivo* and *in vitro*. A: Radial glial cell (type 1 aNSC) labelled with Split-Cre virus 28 days post injection in CAG CAT GFP reporter mice. Scale bar = 20µm. B-C: Representative micrographs (B) and quantification (C) of

recombined Td-Tomato+ cells from *Dicer*$^{wt/wt}$ *Td-Tomato*$^{flox/wt}$ (WT) and *Dicer*$^{flox/flox}$ *Td-Tomato*$^{flox/wt}$ (KO) mice co-expressing Nestin (upper panel), SOX2 (middle panel) or GS (bottom panel) 2 months after Split-Cre virus injections. Data expressed as mean +/-SEM. N= 4-6 mice per group. Scale bar = 20µm. Unpaired-*t-test* *$p < 0.05$. D: aNSCs cultured in proliferative conditions express stem cell markers such as SOX2 (i), GFAP (ii) and Nestin (iii). aNSCs do not express markers of glial differentiation such as S100b (iv) and O4 (vii); or markers of neuronal differentiation such as DCX (v) and Tuj1 (vi). Mouse Adult Neurons show the staining for DCX (viii) and Tuj1 (ix) as positive controls. Scale bar = 50µm.

Figure S2. Related to Figure 2 and Figure 3.

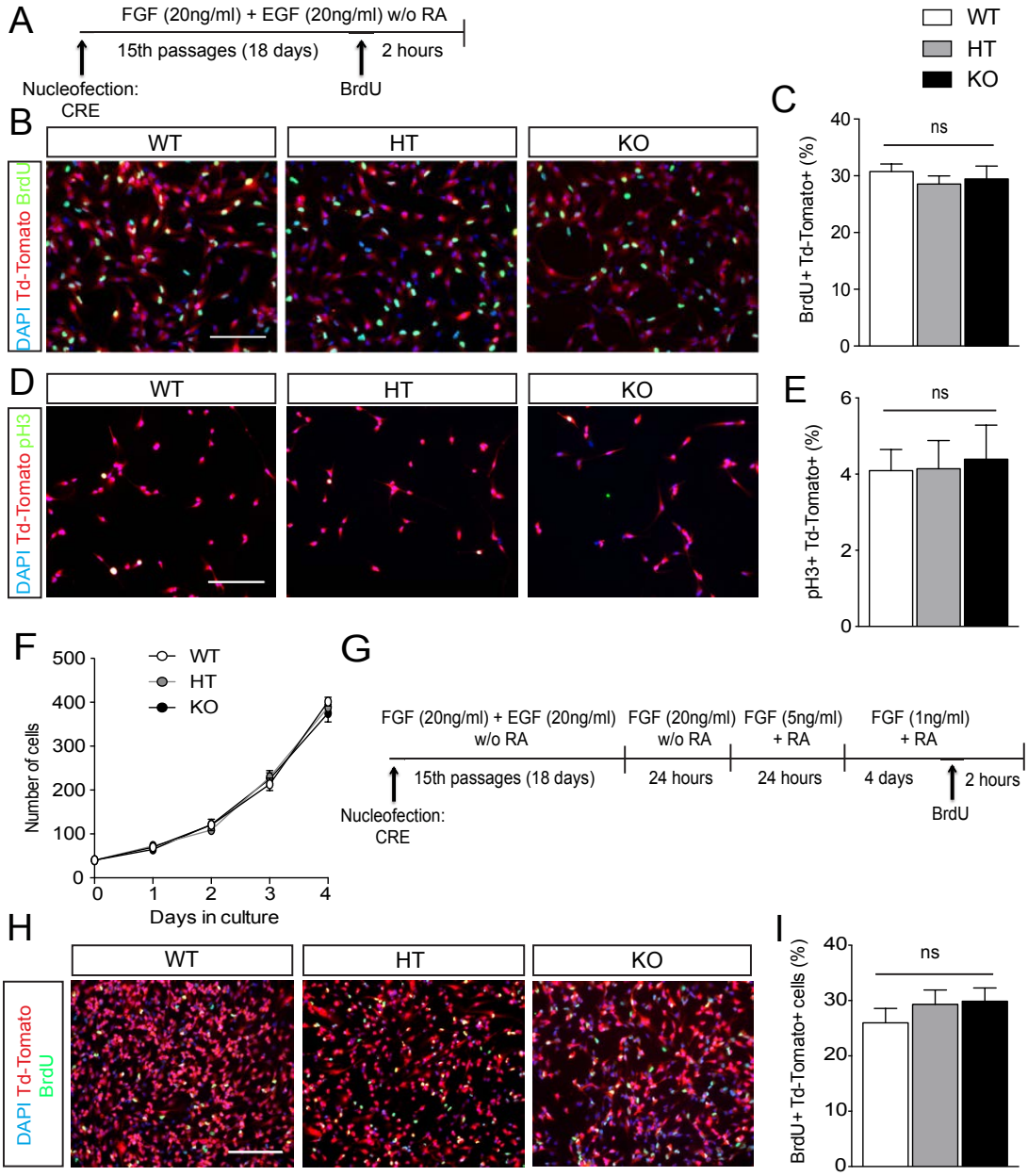

Figure S2. Dicer/miRNA depletion does not affect aNSCs proliferation *in vitro*. A: Schematic representation of the procedure used to assess proliferation after Dicer ablation. B and D: Representative micrographs showing Td-Tomato+ aNSCs from *Dicer*$^{wt/wt}$ *Td-Tomato*$^{flox/wt}$ (WT), *Dicer*$^{flox/wt}$ *Td-Tomato*$^{flox/wt}$ (HT) and *Dicer*$^{flox/flox}$ *Td-Tomato*$^{flox/wt}$ (KO) mice expressing BrdU (B and H) or pH3 (D). C and E: Percentage of Td-Tomato+ cells expressing BrdU after a 2 hours pulse (C) or pH3 (E). F: Growth curve representing the number of cells per field along days of aNSCs under proliferating conditions. G: Schematic representation of the procedure used to assess proliferation under differentiating conditions. I: Percentage of Td-Tomato+ cells expressing BrdU. Scale bar = 50µm. Data expressed as mean +/-SEM. N= 3 independent experiments containing 3 replicates. One-way ANOVA Bonferroni as *post-hoc*.

Figure S3. Related to Figure 2.

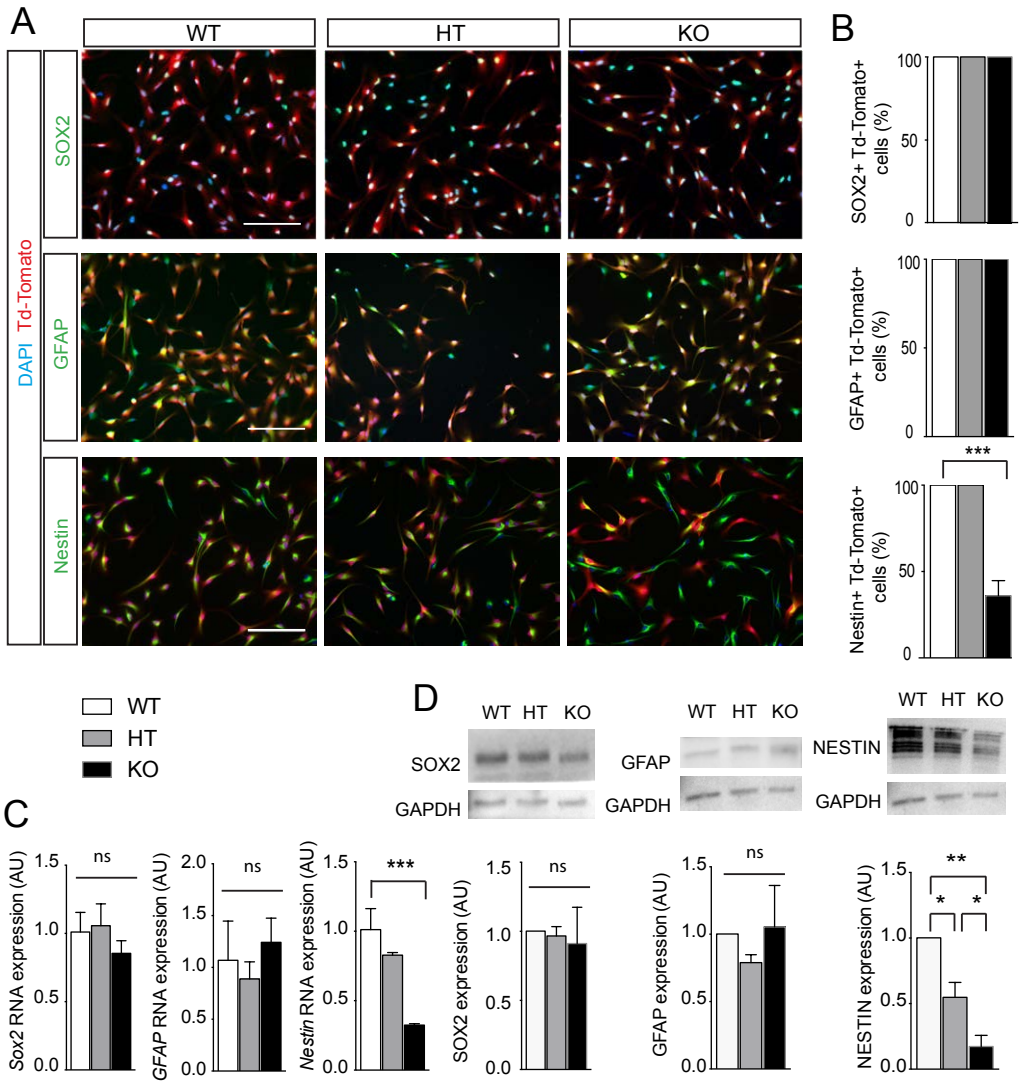

Figure S3. Dicer/miRNA depletion does not affect the expression of aNSCs markers Sox2 and GFAP but impairs Nestin expression *in vitro*. A: Representative micrographs showing recombined aNSCs (Td-Tomato+) from *Dicer*$^{wt/wt}$ *Td-Tomato*$^{flox/wt}$ (WT), *Dicer*$^{flox/wt}$ *Td-Tomato*$^{flox/wt}$ (HT) and *Dicer*$^{flox/flox}$ *Td-Tomato*$^{flox/wt}$ (KO) mice expressing SOX2 (upper panels), GFAP (middle panels) and Nestin (bottom panels). B: Percentage of Td-Tomato+ cells expressing aNSCs markers (SOX2, GFAP and Nestin). C: Relative *Sox2*, *GFAP* and *Nestin* mRNA quantification with qPCR from recombined aNSCs. D: SOX2, GFAP and NESTIN protein quantification from recombined aNSCs cultures. Scale bar = 50µm. Data expressed as mean +/-SEM. N= 3 independent experiments containing 3 replicates. One-way ANOVA Bonferroni as *post-hoc* * $p < 0.05$; ** $p < 0.01$; *** $p < 0.001$

Figure S4. Related to Figure 3.

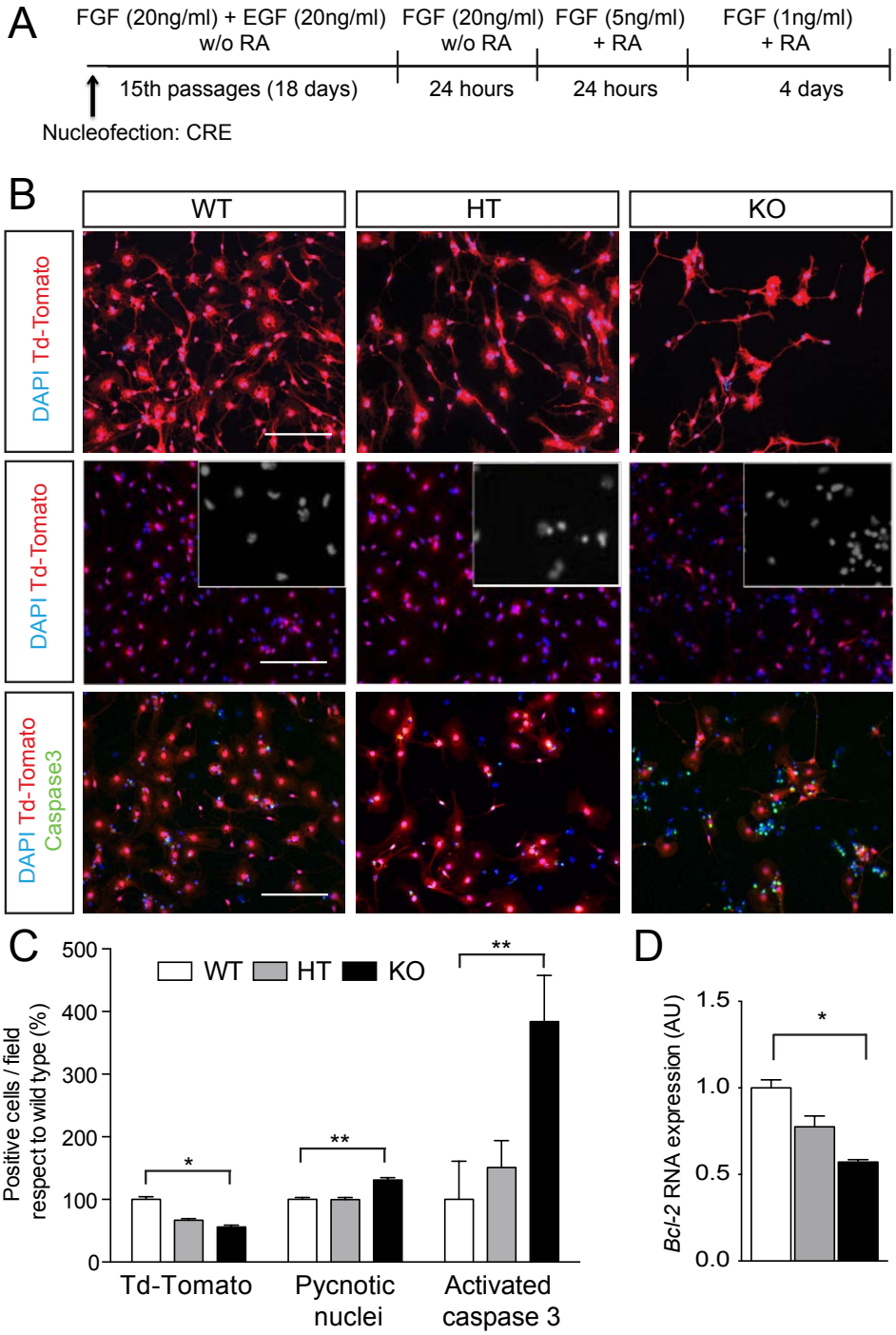

Figure S4. *Dicer*/miRNA depletion increases apoptosis of hippocampal aNSCs upon differentiation *in vitro*. A: Schematic representation of the procedure used to assess survival after Dicer ablation. B: Representative micrographs showing Td-Tomato+ aNSCs after 6 DIV with growth factors titration from *Dicer*$^{wt/wt}$ *Td-Tomato*$^{flox/wt}$ (WT), *Dicer*$^{flox/wt}$ *Td-Tomato*$^{flox/wt}$ (HT) and *Dicer*$^{flox/flox}$ *Td-Tomato*$^{flox/wt}$ (KO) mice that are surviving (upper pannels), dying with pycnotic nuclei (middle pannels) and expressing activated caspase 3 (bottom panels). C: Percentage of Td-Tomato+ cells, pycnotic nuclei and Td-Tomato+ cells expressing activated caspase 3 per field normalized per WT aNSCs after 6DIV. D: Relative *Bcl-2* mRNA quantification with qPCR from recombined aNSCs after 6DIV. Scale bar = 50µm. Data expressed as mean +/-SEM. N= 3 independent experiments containing 3 replicates. One-way ANOVA Bonferroni as *post-hoc* *p < 0.05; **p < 0.01; ***p < 0.001.

Figure S5. Related to Figure 5.

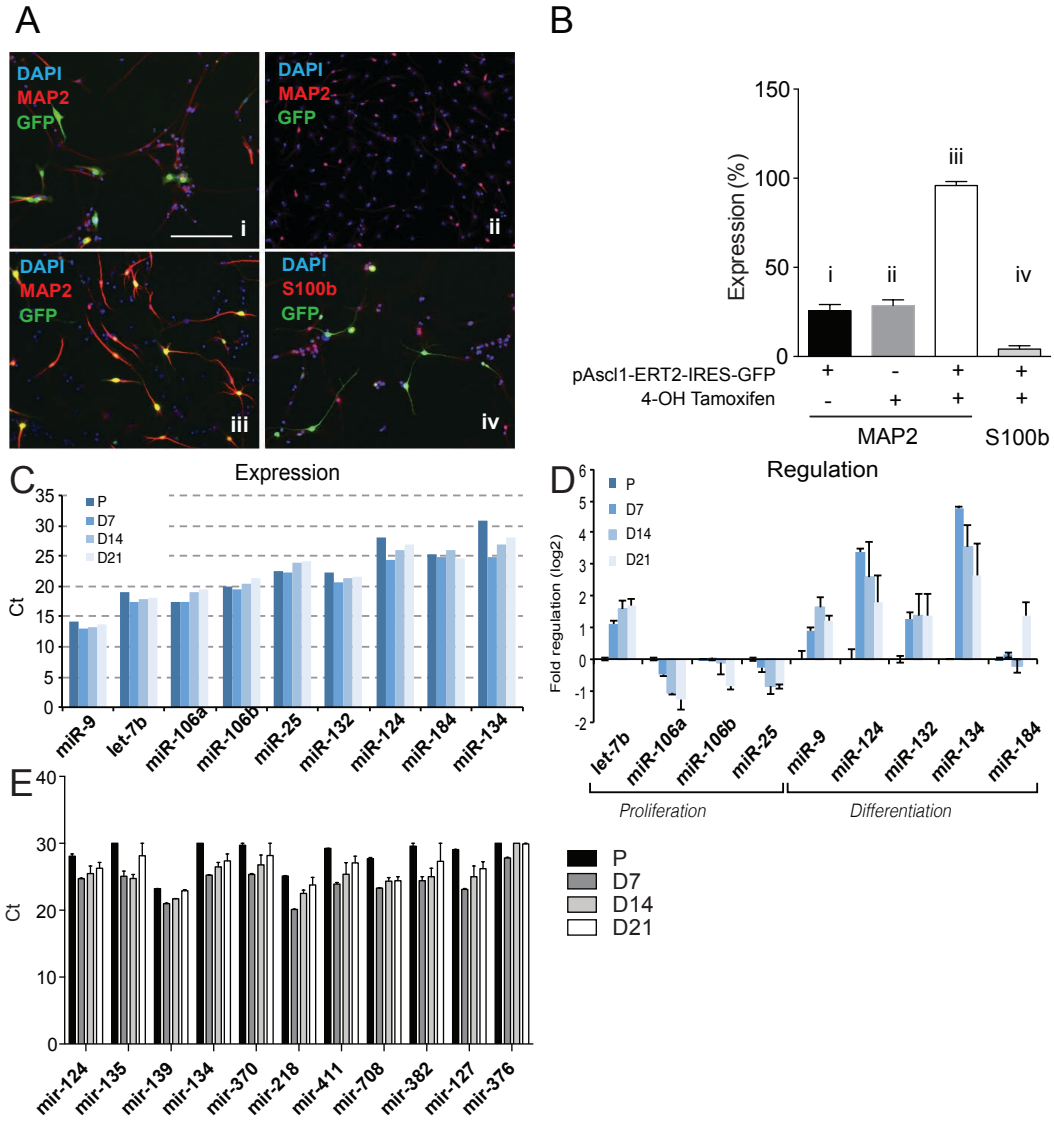

Figure S5. Expression of neurogenesis-induced miRNAs in differentiated hippocampal aNSCs using an inducible retrovirus expressing Ascl1 (*Ascl1-ERT2-IRES-GFP*). After 6 DIV, upon 4-OH tamoxifen administration, 95% of infected cells (GFP+) differentiate to neurons. A: Representative micrographs showing the efficiency of neuronal differentiation upon Ascl1 expression in hippocampal aNSCs at 6 DIV. B: Percentage of MAP2 or S100b expressing cells respect to GFP+ infected cells (i, iii and iv) or DAPI (ii) under different conditions at 6 DIV. Scale bar = 50µm. C: Expression levels of miRNAs known to be involved on neurogenesis as reported by Schouten et al., 2012. D: Fold regulation of known miRNAs during neuronal differentiation. E: Expression levels of selected miRNAs in this study during proliferation (P) or differentiation after 7 (D7), 14 (D14) and 21 (D21) DIVs. Data expressed as mean +/-SEM. N= 3 independent experiments containing 3 replicates.

Figure S6. Related to Figure 6.

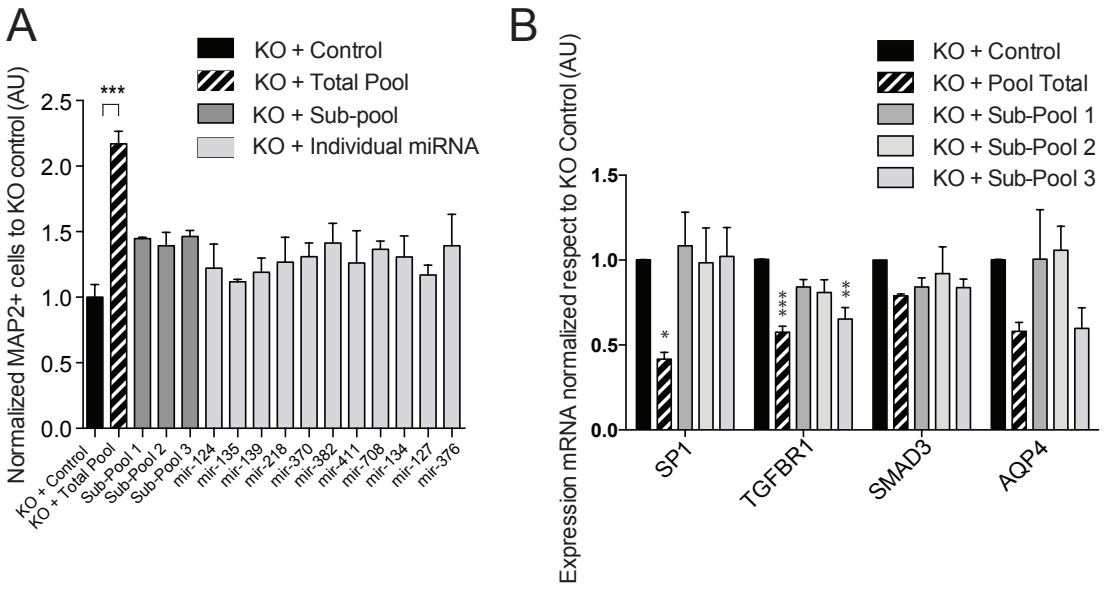

Figure S6. A pool of eleven miRNAs synergistically rescues Dicer-cKO impairment of adult neurogenesis. A: Proportion of KO aNSCs expressing MAP2 upon transfection of 250nM of Sub-Pool 1 (220nM scrambled RNA + 25nM mir-124-3p + 25nM mir-135a-5p), 250nM of Sub-Pool 2 (75nM scrambled RNA + 25nM mir-139-5p + 25nM mir-218-5p + 25nM mir-411-5p + 25nM mir-134-5p + 25nM mir-370-3p + 25nM mir-382-5p + 25nM mir-708-5p), 250nM of Sub-Pool 3 (220nM scrambled RNA + 25nM mir-127-3p + 25nM miR-376b-3p), or each miRNA alone (225nM scrambled RNA + 25nM specific miRNA) respect to KO control. B: Expression of mRNA with qPCR of negative regulators of neuronal differentiation or astrocyte inducers from recombined KO aNSCs transfected with 250nM of scrambled RNA, 250nM of Total Pool or Sub-pools after 6 DIV. Data expressed as mean +/-SEM. N= 3 independent experiments containing 3 replicates. One-way ANOVA Bonferroni as *post-hoc* *$p < 0.05$; **$p < 0.01$; ***$p < 0.001$.

Figure S7. Related to Figure 6.

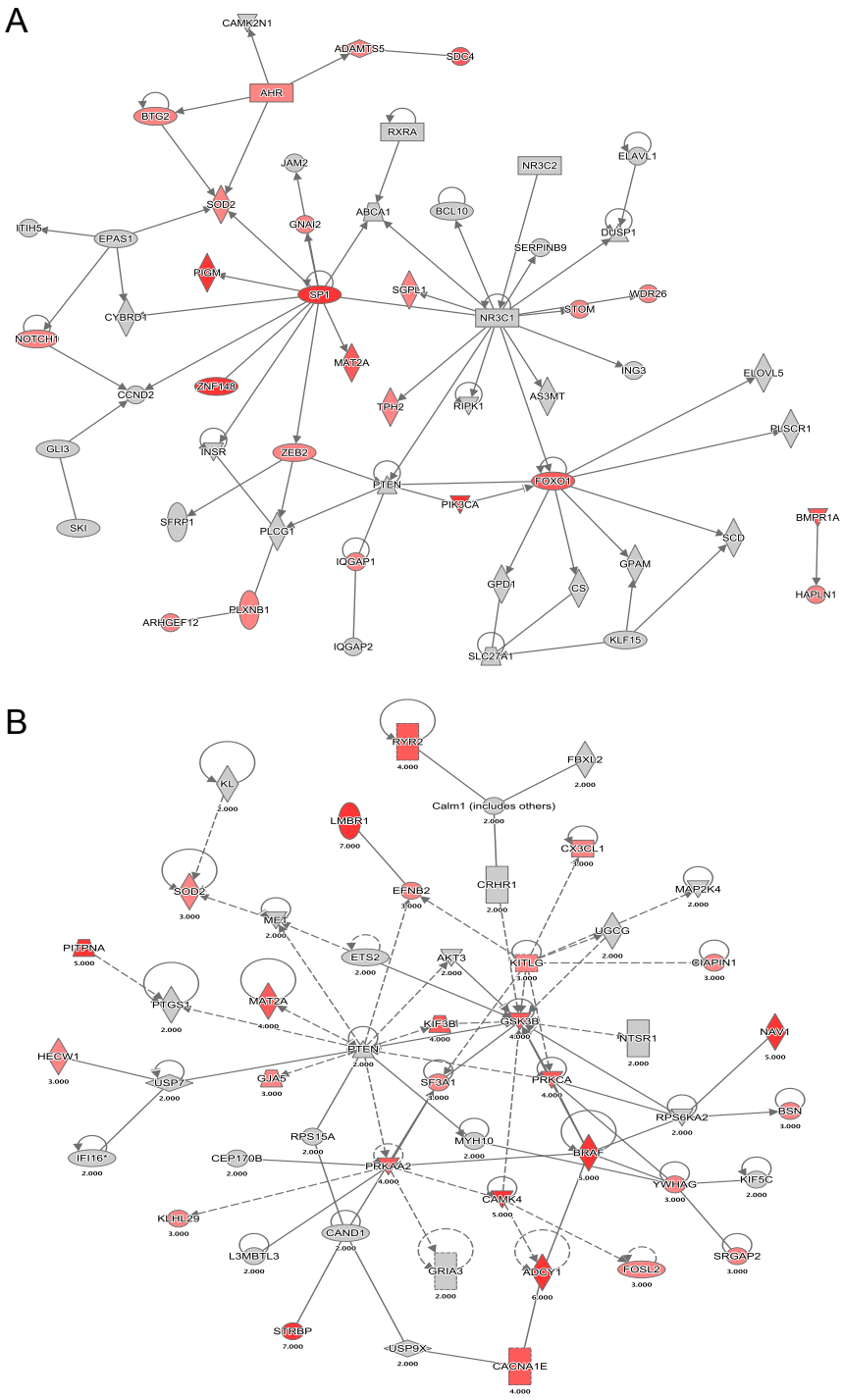

Figure S7. Gene networks of astrocytes and neurons. Representation of connected predicted targets of at least 2 of the eleven miRNAs (previously selected with Mirwalk 2.0) that are a hallmark of astrocytes (A) and neurons (B) as described by Cahoy et al., 2008. Genes targeted by 3 or more miRNAs are indicated in red (more intensity = more miRNAs are targeting the selected gene).

Table S1. Related to Figure 5. Predicted targets of at least two of the eleven miRNAs selected with Mirwalk 2.0.

Table S2. Related to Figure 5. Predicted targets of at least five of the eleven miRNAs selected with Mirwalk 2.0. Predicted targets known to have a role on neuronal and astrocyte differentiation are indicated.

Table S3. Related to Figure 7. Proteomics expression raw data.

Supplemental experimental procedures

Animals

Genotyping of mice carrying the *Dicer*^{flox} allele were performed by PCR following published protocols (Andl et al., 2006); and Td-Tomato according to Jackson laboratories instructions. Animals were 6-8 weeks-old at the time of the Split-Cre viral injections, or 6-8 weeks old for aNSCs preparation.

Virus injection

8 weeks-old mice were anesthetized with isoflurane and 1 µl of virus mix (Split-Cre N-Cre:C-Cre) per DG was stereotaxically injected at the following coordinates: −2.0 anterior/posterior, ±1.6 medial/lateral, and −1.9 to −2.1 dorsal/ventral relative to bregma (in millimeters) as previously described (Beckervordersandforth et al., 2014). One month later, mice received one BrdU intraperitoneal injection per day (50mg/kg) during 5 days. Animals were sacrificed 10 days or 1 month after BrdU injections.

Mice were anesthetized with intraperitoneal administration of ketamine (90mg/kg) and xylazine (5-7mg/kg), and subsequently perfused with PBS followed by 4% paraformaldehyde (PFA). Brains were harversted, postfixed overnight in 4% PFA, and then equilibrated in 30% sucrose. 40 µm brain sections were generated using a sliding microtome and were stored in a −20°C freezer as floating sections in 48 well plates filled with cryoprotectant solution (glycerol, ethylene glycol, and 0.2 M phosphate buffer, pH 7.4, 1:1:2 by volume).

aNSC preparation and culture

DG was isolated from 8-10 mice at the age of 6-8 weeks per genotype for each aNSCs culture preparation. After dissection in Hanks Balanced Salt Solution (HBSS, Gibco) medium, the tissue was enzymatically dissociated with papain (2,5U/ml), dispase (1U/ml) and DNaseI (250U/ml) for 20 min at 37°C. During incubation, the tissue was repeatedly triturated with a fire polished Pasteur pipette. The cell suspension was centrifuged at 130 g for 5 min and the pellet was re-suspended in buffer solution (1x HBSS, 30mM Glucose, 2mM HEPES pH 7,4, 26mM NaHCO3) followed by a centrifugation at 130 g for 5 min. aNSCs were isolated using 22% Percoll gradient solution. After further centrifugation for 5 min at 130 g the cell pellet was re-suspended in 2 ml of culture medium containing Neurobasal (Invitrogen), Glutamax (Invitrogen), 1% penicillin and streptomycin (Invitrogen), B27 without retinoic acid (Invitrogen), FGF (20ng/ml; PeproTech) and EGF (20ng/ml; PeproTech). The dissociated DG tissue was plated into PDL/Laminin (Sigma/Roche) coated wells and incubated at 37°C with 5% CO2. To further remove excess debris, the growth medium was exchanged 24 hours later. Every 2 days half of the growth medium was exchanged with fresh medium to replenish the growth factors. aNSCs were passaged once they reached 80% confluence.

Proliferation medium: Neurobasal, Glutamax, 1% penicillin and streptomycin, B27 without retinoic acid, supplemented with FGF (20ng/ml) and EGF (20ng/ml). 10 µM BrdU (Sigma-Aldrich) was added to aNSCs in proliferation medium 2 hours before fixation.

Neuronal differentiation: aNSCs were plated at 1,2*10E4 cells/cm2 in culture medium supplemented with FGF (20ng/ml) 24 hours. Then medium was exchanged with medium containing B27 with retinoic acid and FGF (5ng/ml) for 24 hours and FGF (1ng/ml) during the next four days. Cells were differentiated in culture for 6 Days in vitro (DIV).

Astrocyte differentiation medium: aNSCs were plated at a density of 1,2*10E4 cells/cm2 in growth medium with 10% FBS without growth factors for 6 DIV.

Retrovirus-mediated inducible neuronal differentiation: viral construct expressing Ascl1-ERT2 and infections conditions were previously described (Braun et al., 2013). Neuronal differentiation was induced by growth factor withdrawal in the presence of 0.5 mM OH-TAM (Sigma) for 2 days. The medium was changed every 2–3 days. Cells were fixed at 7, 14 or 21 days after the exposition to OH-TAM.

MiRNA administration: aNSCs from Dicerflox/flox Td-Tomatoflox/wt (KO) mice were transfected under proliferating conditions using Amaxa (Lonza) with 250nM of scrambled RNA, Total Pool (25nM of each miRNA), 250nM of Sub-Pool 1 (220nM scrambled RNA + 25nM mir-124-3p + 25nM mir-135a-5p), 250nM of Sub-Pool 2 (75nM scrambled RNA + 25nM mir-139-5p + 25nM mir-218-5p + 25nM mir-411-5p + 25nM mir-134-5p + 25nM mir-370-3p + 25nM mir-382-5p + 25nM mir-708-5p), 250nM of Sub-Pool 3 (220nM scrambled RNA + 25nM mir-127-3p + 25nM miR-376b-3p), each miRNA alone (225nM scrambled RNA + 25nM specific miRNA) or a pool of 10 miRNA by the withdrawal of individual miRNAs (25nM scrambled RNA + 225nM of 10 miRNA).

MiRNA mimics used for Nucleofection

miRIDIAN microRNA	Reference Dharmacon
mmu-miR-135a-5p	C-310411-05-0002
mmu-miR-376b-3p	C-310616-07-0002
mmu-miR-139-5p	C-310568-07-0002
mmu-miR-218-5p	C-310576-05-0002
mmu-miR-411-5p	C-310822-01-0002
mmu-miR-127-3p	C-310397-07-0002
mmu-miR-134-5p	C-310409-05-0002
mmu-miR-370-3p	C-310619-07-0002
mmu-miR-382-5p	C-310607-05-0002
mmu-miR-708-5p	C-310987-01-0002
mmu-miR-124-3p	C-310391-05-0002

MiRNA antagomirs used for Nucleofection

miRIDIAN microRNA Harpin Inhibitor	Reference Dharmacon
mmu-miR-135a-5p	IH-310411-07-0002
mmu-miR-376b-3p	IH-310616-08-0002
mmu-miR-139-5p	IH-310568-08-0002
mmu-miR-218-5p	IH-310575-07-0002
mmu-miR-411-5p	IH-310822-02-0002
mmu-miR-127-3p	IH-310397-08-0002
mmu-miR-134-5p	IH-310409-07-0002
mmu-miR-370-3p	IH-310619-08-0002
mmu-miR-382-5p	IH-310607-07-0002
mmu-miR-708-5p	IH-310987-02-0002
mmu-miR-124-3p	IH-310390-07-0002

Immunofluorescence

The immunofluorescence staining on brain slices was performed on sections covering the entire dorsal hippocampus (Bregma, -1.06 to -2.18 mm, Paxinos and Franklin, 2001). Sections were washed with 0.1M PBS during 40 min and pretreated with 2N HCL at 30,2°C for 30 min. After extensive washings with 0.1M PBS, sections were permeabilized with 0.3% PBS-T (PBS-Triton X-100) for 10 min followed with 20 min with 0.1% PBS-T. Sections were blocked during 2 h with 0.1% PBS-T and 5% FBS at room temperature (RT) followed by incubation with primary antibodies in a blocking solution overnight at 4°C. The next day, after washing extensively with 0.1% PBS-T sections were subsequently incubated for 1 h with the corresponding secondary fluorescent antibodies (1/1000; Goat or donkey Alexa 488, 568, and 647nm, Invitrogen). Sections were counterstained with Hoechst (1:300), mounted and cover slipped with mowiol reagent.

The immunofluorescence staining on cell cultures was performed after fixing aNSCs for 30 min with 4% paraformaldehyde (PFA) followed by extensive washings with PBS during 30 min. Cells were washed three times with PBS 0,1% Triton X-100 (PBS-T) and blocked during 2 hours with PBS-T containing 5% normal goat serum (Vector laboratories), followed by overnight incubation with primary antibodies. To detect BrdU incorporation, cells were pretreated with 2M HCl for 30 min at 37°C followed by washing with borate buffer, pH 8.5, for 30 min, before being subjected to immunofluorescence. The next day, after washing extensively with PBS-T, cells were incubated with secondary antibodies. Cells were mounted in mounting medium and counterstained with fluorescent nuclear dye DAPI (Invitrogen).

Primary Antibodies used for immunofluorescence

Antibody	Host	Company	Catalog	Dilution
BrdU	rat	Abcam	ab-6326	1:200
DCX	rabbit	Abcam	ab18723	1:1000
DCX	goat	Santacruz	SC8066	1:200
GFAP	rabbit	Dako	Z-0334	1:1000
S100b	mouse	Sigma	S2532	1:250-1:500
NeuN	mouse	Millipore	MAB377	1:250
GS	mouse	Millipore	MAB302	1:400
SOX2	rabbit	Millipore	AB5603	1:200-1:500
Nestin	mouse	Millipore	MAB353	1:250
Nestin	rat	BD-Pharmigen	556309	1:200
pH3	rat	Abcam	AB10543	1:500

Primers used for gene expression analysis by quantitative PCR

Primer Name	Sequence
Actin Fw	GGCTGTATTCCCCTCCATCG
Actin Rv	CCAGTTGGTAACAATGCCATGT
Aqp4 Fw	GAGTCACCACGGTTCATGGA
Aqp4 Rv	CGTTTGGAATCACAGCTGGC
Bcl-2 Fw	GGTATGCACCCAGAGTGATGC
Bcl-2 Rv	ATGCCTTTGTGGAACTATATGGC
Dicer Fw	CCTGACAGTGACGGTCCAAAG
Dicer Fw 2	GGAACGCTAACACATCTACCT
Dicer Rv	CATGACTCTTCAACTCAAACT
Dicer Rv 2	AGAGTCCATCCTGTCCTTGA
GAPDH Fw	TGCACCACCAACTGCTTAGC
GAPDH Rv	GGCATGGACTGTGGTCATGAG
GFAP Fw	GGGGCAAAAGCACCAAAGAAG
GFAP Rv	GGGACAACTTGTATTGTGAGCC
Nestin Fw	CCCTGAAGTCGAGGAGCTG
Nestin Rv	CTGCTGCACCTCTAAGCGA
S100b Fw	CTGGAGAAGGCCATGGTTGC
S100b Rv	CTCCAGGAAGTGAGAGAGCT
Smad3 Fw	CTGGGCCTACTGTCCAATGT
Smad3 Rv	CATCTGGGTGAGGAC CTTGT
Sp1 Fw	GGCAATAATGGGGGTAGCGG
Sp1 Rv	CAAGCTGGCAGAACTGATGGC
Tgfbr1 Fw	CATTCACCACCGTGTGCCAAATGA
Tgfbr1 Rv	ACCTGATCCAGACCCTGATGTTGT

Quantification of miRNAs

MiRNA profiling was performed on 200 ng of total RNA for each sample and Megaplex reactions were run with 12 cycles of pre-amplification. PreAmp products were diluted 1:4 in TE and 9 µl of the diluted reactions were loaded on microRNA cards. Arrays were run on a ViiA 7 Real-Time PCR system (Thermo Fisher). Raw data were exported to excel to be further analyzed. First, miRNA expression was normalized by using scaling factors calculated by median-centering the Cq values of the house-keeping genes included in each array (namely: U6, sno135, sno202, U87 and Y1). Undetermined values or Cq values >30.01 were arbitrarily set to 30.01, without any further normalization. Next, the scaled Cq values were centered on the median expression over all samples (Proliferating aNSCs, differentiating at DIV7, DIV14, DIV21). These values were used for hierarchical clustering analysis in Figure 6.

MiRNA quantification from FACS sorted Td-Tomato+ cells two months after the Split-Cre injection in WT and Dicer cKO mice was performed using the miScript Primer Assay (Qiagen) following the manufacturer's instructions.

***In silico* analysis**

Predicted target analysis was performed with the miRWalk 2.0 platform with highly restrictive parameters: seed sequence length of 7 bp, p value <0.01 and predicted targets for at least 8 databases including *miRWalk, MicroT4, miRanda, miRBridge, miRDB, miRMap, miRNAMap, PICTAR2, PITA, RNA22, RNAhybrid* and *Targetscan*).

Gene Ontology (GO) analysis was performed with DAVID Bioinformatics Resources v6.8 to classify the significantly dysregulated proteins into biological processes (BP).

Expression proteomics experiments

Sample preparation

Transfected WT aNSCs with a pool of miRNA inhibitors (250nM) or control RNA were collected after 6 DIV in differentiation conditions (3 independent experiments). At the end of the experiment, cells where lysed with RIPA buffer and 60ug of proteins were collected from all the samples to isobarically label them using TMT sixplex kits (Thermofisher Scientific) following the protocol suggested by the vendor. Tags 126 to 128 *m/z* were used for the control samples (3 replicates); tags 129 to 131 *m/z* were used for the miRNA inhibitor treated samples (3 replicates). Briefly, samples were reduced with dithiothreitol (DTT), alkylated with iodoacetamide (IAA) and then labeled using the TMT tags. After pooling the six conditions, half of the total protein content (180ug) was loaded on a monodimensional

gel-electrophoresis (1DGE). The whole lane was then cut into 12 slices and in-gel protein digestion was performed, according to (Shevchenko et al., 2006). The recovered samples were dried under nitrogen steam then re-dissolved with 50ul of 3% acetonitrile (ACN) with 0.1% formic acid for LC-MS/MS analysis.

LC-MS/MS analysis

The tryptic peptide mixture was analyzed using a Synapt G2 QToF instrument equipped with nanoACQUITY liquid chromatographer and a nanoSpray ion source. Peptides were separated on a BEH nanobore column (75um IDX25cm length) using a linear gradient of ACN in water from 3 to 55% in three hours, followed by a washout step at 90%ACN (10 min) and a reconditioning step to 3% for 20 min. Flow rate was set to 300 nL/min. Spray voltage was set to 1.6kV, cone voltage was set to 28V, spray gas was set to 0.3 L/min. Survey spectra were acquired over the 50-1600 *m/z* scan range. Multiply charged ions (2+,3+ and 4+) between 300 and 1400 *m/z* were selected as precursors for Data Dependent Acquisition (DDA) tandem mass analysis and fragmented in the Trap region of the instrument. Collision energy (CE) values were automatically selected by the software using dedicated charge-state dependent CE/*m/z* profiles. Every 60 seconds a single LeuEnk (2ng/ml) MS scan was acquired by the LockMass ion source for spectra recalibration.

Data analysis

Acquired raw datafiles were processed using PLGS software (Waters Inc.) to recalibrate the mass spectra and to generate the precursor-fragment peaklist. Protein identification and quantification were performed by interrogating the SwissProt database using MASCOT Server software (Matrixscience) (Shevchenko et al., 2006). The search parameters were set as follows, quantification: TMT6plex; fixed modifications: carbamidomethyl (C), TMT6plex (K); variable modifications: acetyl (K), acetyl (N-term), TMT6plex (N-terminus); deamidated (NQ), methyl (DE), oxidation (M), phospho (ST), phospho (Y); peptide tolerance: 50ppm; fragment tolerance: 0.5Da; maximum allowed missed cleavages: 2. At least 2 peptides were required for a positive protein identification and quantification. Protein expression ratio was normalized by the average ratio off all the peptides assigned to proteins.

Supplemental references

Andl, T., Murchison, E.P., Liu, F., Zhang, Y., Yunta-Gonzalez, M., Tobias, J.W., Andl, C.D., Seykora, J.T., Hannon, G.J., and Millar, S.E. (2006). The miRNA-processing enzyme dicer is essential for the morphogenesis and maintenance of hair follicles. Curr. Biol. CB 16, 1041–1049.

Chuikov, S., Levi, B.P., Smith, M.L., and Morrison, S.J. (2010). Prdm16 promotes stem cell maintenance in multiple tissues, partly by regulating oxidative stress. Nat. Cell Biol. 12, 999–1006.

Deneen, B., Ho, R., Lukaszewicz, A., Hochstim, C.J., Gronostajski, R.M., and Anderson, D.J. (2006). The transcription factor NFIA controls the onset of gliogenesis in the developing spinal cord. Neuron 52, 953–968.

Dweep, H et al. miRWalk2.0: a comprehensive atlas of microRNA-target interactions, Nature Methods, 12(8): 697-697 (2015).

Guadaño-Ferraz, A., Obregón, M.J., Germain, D.L.S., and Bernal, J. (1997). The type 2 iodothyronine deiodinase is expressed primarily in glial cells in the neonatal rat brain. Proc. Natl. Acad. Sci. U. S. A. 94, 10391–10396.

Huang, Y.-C., Shih, H.-Y., Lin, S.-J., Chiu, C.-C., Ma, T.-L., Yeh, T.-H., and Cheng, Y.-C. (2015). The epigenetic factor Kmt2a/Mll1 regulates neural progenitor proliferation and neuronal and glial differentiation. Dev. Neurobiol. 75, 452–462.

Kaul, A., Chen, Y.-H., Emnett, R.J., Gianino, S.M., and Gutmann, D.H. (2013). Conditional KIAA1549:BRAF mice reveal brain region- and cell type-specific effects. Genes. N. Y. N 2000 51, 708–716.

Li, X., Law, J.W.S., and Lee, A.Y.W. (2012). Semaphorin 5A and plexin-B3 regulate human glioma cell motility and morphology through Rac1 and the actin cytoskeleton. Oncogene 31, 595–610.

Michinaga, S., Ishida, A., Takeuchi, R., and Koyama, Y. (2013). Endothelin-1 stimulates cyclin D1 expression in rat cultured astrocytes via activation of Sp1. Neurochem. Int. 63, 25–34.

Olsen, M.L., and Sontheimer, H. (2008). Functional implications for Kir4.1 channels in glial biology: from K+ buffering to cell differentiation. J. Neurochem. 107, 589–601.

Paxinos G, Franklin KBJ (2001) The Mouse Brain in Stereotaxic Coordinates: Second Edition. Elsevier Academic Press, San Diego, CA. 10.1111/j.1469–7580.2004.00264.x.

Shen, T., Sun, C., Zhang, Z., Xu, N., Duan, X., Feng, X.-H., and Lin, X. (2014). Specific control of BMP signaling and mesenchymal differentiation by cytoplasmic phosphatase PPM1H. Cell Res. 24, 727–741.

Sim, F.J., McClain, C., Schanz, S., Protack, T.L., Windrem, M.S., and Goldman, S.A. (2011). CD140a identifies a population of highly myelinogenic, migration-competent, and efficiently engrafting human oligodendrocyte progenitor cells. Nat. Biotechnol. 29, 934–941.

Stipursky, J., and Gomes, F.C.A. (2007). TGF-β1/SMAD signaling induces astrocyte fate commitment in vitro: Implications for radial glia development. Glia 55, 1023–1033.

Sun, M., Forsman, C., Sergi, C., Gopalakrishnan, R., O'Connor, M.B., and Petryk, A. (2010). The expression of Twisted gastrulation in postnatal mouse brain and functional implications. Neuroscience 169, 920–931.

Zeng, X.-N., Sun, X.-L., Gao, L., Fan, Y., Ding, J.-H., and Hu, G. (2007). Aquaporin-4 deficiency down-regulates glutamate uptake and GLT-1 expression in astrocytes. Mol. Cell. Neurosci. 34, 34–39.

Zhang, Y., Zhang, J., Navrazhina, K., Argaw, A.T., Zameer, A., Gurfein, B.T., Brosnan, C.F., and John, G.R. (2010). TGFbeta1 induces Jagged1 expression in astrocytes via ALK5 and Smad3 and regulates the balance between oligodendrocyte progenitor proliferation and differentiation. Glia 58, 964–974

Table S2. Predicted targets of at least five of the eleven miRNAs selected with Mirwalk 2.0. Related to Figure 5.

Predicted targets of > 5 miRNAs												
Gene name	**mmu-miR-124-3p**	**mmu-miR-127-3p**	**mmu-miR-135a-5p**	**mmu-miR-134-5p**	**mmu-miR-139-5p**	**mmu-miR-218-5p**	**mmu-miR-370-3p**	**mmu-miR-382-5p**	**mmu-miR-411-5p**	**mmu-miR-708-5p**	**mmu-miR-376b-3p**	**Number of miRNAs**
Adcy1	Adcy1		Adcy1		Adcy1	Adcy1	Adcy1	Adcy1				6
Afap1	Afap1		Afap1				Afap1		Afap1	Afap1		5
Amotl1	Amotl1			Amotl1		Amotl1	Amotl1			Amotl1		5
Aqp4			Aqp4			Aqp4	Aqp4	Aqp4		Aqp4	Aqp4	6
Arhgef6	Arhgef6		Arhgef6				Arhgef6	Arhgef6			Arhgef6	5
Arih1	Arih1		Arih1		Arih1			Arih1		Arih1		5
Bcl2l13	Bcl2l13				Bcl2l13			Bcl2l13	Bcl2l13	Bcl2l13		5
Braf	Braf			Braf		Braf		Braf		Braf		5
Camk4				Camk4	Camk4	Camk4	Camk4				Camk4	5
Cask	Cask					Cask	Cask	Cask		Cask		5
Cntn2	Cntn2		Cntn2			Cntn2	Cntn2			Cntn2	Cntn2	6
Coa5			Coa5	Coa5	Coa5	Coa5				Coa5		5
Csnk1g1			Csnk1g1		Csnk1g1		Csnk1g1		Csnk1g1	Csnk1g1		5
D430041D05Rik			D430041D05Rik		D430041D05Rik		D430041D05Rik	D430041D05Rik		D430041D05Rik		5
Dcbld2				Dcbld2	Dcbld2	Dcbld2			Dcbld2	Dcbld2		5
Ddx3x	Ddx3x		Ddx3x		Ddx3x		Ddx3x	Ddx3x				5
Dhfr	Dhfr			Dhfr		Dhfr	Dhfr				Dhfr	5
Dio2	Dio2		Dio2	Dio2				Dio2	Dio2	Dio2		6
Dock5	Dock5		Dock5	Dock5		Dock5			Dock5	Dock5		6
Eif5b			Eif5b				Eif5b	Eif5b		Eif5b	Eif5b	5
Eri1			Eri1		Eri1		Eri1		Eri1	Eri1		5
Faf2	Faf2				Faf2	Faf2	Faf2			Faf2		5
Fut9			Fut9		Fut9	Fut9		Fut9	Fut9		Fut9	6
Gm608			Gm608	Gm608	Gm608		Gm608			Gm608		5
Grk1			Grk1	Grk1	Grk1		Grk1			Grk1		5
Homer2	Homer2				Homer2		Homer2	Homer2			Homer2	5
Hook3	Hook3		Hook3	Hook3		Hook3	Hook3	Hook3		Hook3		7
Hs3st3b1				Hs3st3b1	Hs3st3b1	Hs3st3b1	Hs3st3b1	Hs3st3b1				5
Hus1				Hus1		Hus1	Hus1	Hus1		Hus1		5
Iws1	Iws1			Iws1			Iws1		Iws1	Iws1	Iws1	6
Kcna1	Kcna1			Kcna1	Kcna1	Kcna1	Kcna1				Kcna1	6
Kcnc1	Kcnc1			Kcnc1	Kcnc1	Kcnc1	Kcnc1			Kcnc1	Kcnc1	7
Kmt2a	Kmt2a		Kmt2a			Kmt2a	Kmt2a		Kmt2a			5
Limd2	Limd2				Limd2	Limd2	Limd2	Limd2				5
Lmbr1				Lmbr1		Lmbr1	Lmbr1	Lmbr1	Lmbr1	Lmbr1	Lmbr1	7
Lpar2			Lpar2	Lpar2	Lpar2	Lpar2	Lpar2					5
Lpp	Lpp		Lpp		Lpp		Lpp			Lpp	Lpp	6
Lrrc15		Lrrc15	Lrrc15	Lrrc15	Lrrc15		Lrrc15					5
Luzp1	Luzp1			Luzp1	Luzp1		Luzp1			Luzp1		5
Man2a1	Man2a1		Man2a1			Man2a1				Man2a1	Man2a1	5
Map3k1	Map3k1				Map3k1		Map3k1		Map3k1	Map3k1		5
Mat2a	Mat2a		Mat2a	Mat2a	Mat2a					Mat2a		5
Mtmr1			Mtmr1			Mtmr1		Mtmr1		Mtmr1	Mtmr1	5
Nfib	Nfib			Nfib	Nfib			Nfib			Nfib	5
Pcnx	Pcnx				Pcnx		Pcnx	Pcnx		Pcnx		5
Pdpk1	Pdpk1				Pdpk1		Pdpk1	Pdpk1		Pdpk1		5
Pdzd2				Pdzd2		Pdzd2	Pdzd2			Pdzd2	Pdzd2	5
Pigm			Pigm		Pigm	Pigm		Pigm		Pigm		5
Pik3c2a	Pik3c2a		Pik3c2a	Pik3c2a		Pik3c2a			Pik3c2a			5
Pitpna	Pitpna			Pitpna	Pitpna		Pitpna			Pitpna		5
Ppm1h	Ppm1h		Ppm1h	Ppm1h			Ppm1h	Ppm1h				5

Ppp1r9a			Ppp1r9a		Ppp1r9a	Ppp1r9a	Ppp1r9a	Ppp1r9a		Ppp1r9a		6
Prdm16		Prdm16	Prdm16		Prdm16	Prdm16	Prdm16		Prdm16			6
Prkca	Prkca			Prkca	Prkca		Prkca	Prkca				5
Ptpn14	Ptpn14		Ptpn14	Ptpn14	Ptpn14		Ptpn14	Ptpn14	Ptpn14	Ptpn14		8
Rab6b			Rab6b		Rab6b		Rab6b	Rab6b		Rab6b		5
Sema3d			Sema3d	Sema3d	Sema3d	Sema3d		Sema3d				5
Sema5a	Sema5a		Sema5a		Sema5a	Sema5a			Sema5a	Sema5a		6
Sertad2	Sertad2		Sertad2	Sertad2		Sertad2	Sertad2					5
Sertad4	Sertad4		Sertad4			Sertad4	Sertad4			Sertad4		5
Setd7	Setd7		Setd7		Setd7		Setd7			Setd7	Setd7	6
Slc44a5	Slc44a5		Slc44a5	Slc44a5	Slc44a5					Slc44a5		5
Slc4a8	Slc4a8		Slc4a8	Slc4a8	Slc4a8					Slc4a8	Slc4a8	6
Slc5a3	Slc5a3				Slc5a3	Slc5a3	Slc5a3	Slc5a3		Slc5a3		6
Slc7a14	Slc7a14		Slc7a14	Slc7a14		Slc7a14				Slc7a14		5
Smad3		Smad3	Smad3		Smad3		Smad3			Smad3		5
Smcr8	Smcr8			Smcr8		Smcr8	Smcr8			Smcr8		5
Sp1	Sp1		Sp1	Sp1		Sp1				Sp1		5
Srp54b	Srp54b		Srp54b			Srp54b	Srp54b	Srp54b				5
Sspn	Sspn		Sspn		Sspn	Sspn		Sspn				5
Ssr1			Ssr1	Ssr1		Ssr1	Ssr1		Ssr1			5
St8sia1	St8sia1			St8sia1			St8sia1		St8sia1	St8sia1	St8sia1	6
Stk38l			Stk38l			Stk38l	Stk38l	Stk38l		Stk38l	Stk38l	6
Tbl1xr1			Tbl1xr1	Tbl1xr1		Tbl1xr1		Tbl1xr1			Tbl1xr1	5
Tgfbr1	Tgfbr1		Tgfbr1					Tgfbr1	Tgfbr1	Tgfbr1		5
Tnrc6b	Tnrc6b			Tnrc6b	Tnrc6b	Tnrc6b	Tnrc6b					5
Tspan11	Tspan11			Tspan11	Tspan11	Tspan11	Tspan11			Tspan11		6
Twsg1	Twsg1		Twsg1		Twsg1	Twsg1	Twsg1	Twsg1				6
Ubn2	Ubn2				Ubn2	Ubn2	Ubn2			Ubn2		5
Xpo7			Xpo7	Xpo7	Xpo7	Xpo7				Xpo7		5
Zdhhc21			Zdhhc21	Zdhhc21	Zdhhc21				Zdhhc21	Zdhhc21		5
Zfand3	Zfand3	Zfand3			Zfand3		Zfand3	Zfand3				5
Zfp148					Zfp148		Zfp148		Zfp148	Zfp148	Zfp148	5
Zfp275	Zfp275		Zfp275	Zfp275			Zfp275				Zfp275	5
Zfp704	Zfp704		Zfp704		Zfp704		Zfp704	Zfp704				5
Zfyve27	Zfyve27		Zfyve27	Zfyve27	Zfyve27					Zfyve27		5
Zkscan8	Zkscan8				Zkscan8	Zkscan8	Zkscan8			Zkscan8		5
Zmat3	Zmat3		Zmat3	Zmat3	Zmat3				Zmat3			5

Genes involved in neurogenesis or gliogenesis predicted targets of > 5 miRNAs												
Gene name	**mmu-miR-124-3p**	**mmu-miR-135a-5p**	**mmu-miR-382-5p**	**mmu-miR-134-5p**	**mmu-miR-411-5p**	**mmu-miR-218-5p**	**mmu-miR-370-3p**	**mmu-miR-708-5p**	**mmu-miR-139-5p**	**mmu-miR-376b-3p**	**mmu-miR-127-3p**	**References**
Aqp4		Aqp4	Aqp4			Aqp4	Aqp4	Aqp4		Aqp4		Zeng et al., 2007
Braf	Braf		Braf	Braf		Braf		Braf				Kaul et al., 2013
Dio2	Dio2	Dio2	Dio2	Dio2	Dio2			Dio2				Guadaño-Ferraz et al., 1997
Kcna1	Kcna1			Kcna1		Kcna1	Kcna1		Kcna1	Kcna1		Olsen and Sontheimer, 2008
Kmt2a	Kmt2a	Kmt2a			Kmt2a	Kmt2a	Kmt2a					Huang et al., 2015
Nfib	Nfib		Nfib	Nfib					Nfib	Nfib		Deneen et a., 2006
Ppm1h	Ppm1h	Ppm1h	Ppm1h	Ppm1h			Ppm1h					Shen et al., 2014
Prdm16		Prdm16			Prdm16	Prdm16	Prdm16		Prdm16		Prdm16	Chuikov et al., 2010
Sema5a	Sema5a	Sema5a			Sema5a	Sema5a		Sema5a	Sema5a			Li et al., 2012
Smad3		Smad3					Smad3	Smad3	Smad3		Smad3	Zhang et al., 2010
Sp1	Sp1	Sp1		Sp1		Sp1		Sp1				Michinaga et al., 2013
St8sia1	St8sia1			St8sia1	St8sia1		St8sia1	St8sia1		St8sia1		Sim et al., 2011
Tgfbr1	Tgfbr1	Tgfbr1	Tgfbr1		Tgfbr1			Tgfbr1				Stipursky et al., 2007
Twsg1	Twsg1	Twsg1	Twsg1			Twsg1	Twsg1		Twsg1			Sun et al., 2010
Number predicted targets	11	10	7	7	6	8	8	8	6	4	2	